Consequences of the multichannel structure of soil food webs on ecosystem functioning

P. Quévreux, Franck Jabot

Consequences of the multichannel structure of soil food webs on ecosystem functioning

Pierre Quévreux[1] and Franck Jabot[1]

[1] *Unité Mixte de Recherche sur l'Ecosystème Prairial (UREP - UMR 0874), INRAE-VetAgro Sup, 5 chemin de Beaulieu, 63000 Clermont-Ferrand, France*

Key words: carbon cycling, soil respiration, soil invertebrates, microbivores, decomposition, organic matter

Authors:

- pierre.quevreux@cri-paris.org (corresponding)
- franck.jabot@inrae.fr

Abstract

Soil fauna significantly contributes to carbon cycle but has been neglected in most soil ecosystem models. Soil food webs have been empirically described as a micro-food web relying on microbial production plus a macro-food web relying on detritivorous invertebrates. To understand the consequences of such a structure on ecosystem functioning, we built two models harbouring either a multichannel structure or a purely size-dependent trophic structure representative of classic food web theory. We found that the multichannel structure successfully predicts the empirical relationship between body sizes and trophic levels in soils, and the biomass distribution among the main invertebrate trophic groups. Both models predict a major contribution of microbivores (e.g. protists) to the total ecosystem respiration contrary to previous estimations, which underlines the potentially high impact of microfauna on the carbon cycle. Our model represents a milestone to link the trophic dynamics of soil fauna to ecosystem functioning and biogeochemical cycles.

Introduction

Soils ensure services of first importance to face the global change challenges. The storage of carbon promoted by the 4 per 1000 initiative (Minasny et al., 2017) or the fertility of croplands depend on the tight interactions between biological activity and biogeochemical cycles (Crowther et al., 2019). Soil fauna processes a biomass equivalent of up to 90% of primary production (Cebrian, 1999) and plays a key role in biogeochemical cycles. In particular, detritivorous invertebrates consume up to 100% of the annual litter fall (Heděnec et al., 2022) and strongly enhance the decomposition of plant litter by shredding the fresh organic matter into pieces (Wall et al., 2008), which increases its degradability by microbes (Joly et al., 2020; Coq et al., 2022). Nevertheless, the majority of models assessing the functioning of soil ecosystems only consider micro-organisms (Wieder et al., 2013; Perveen et al., 2014), because of their overwhelming biomass compared to soil fauna. The repeated calls to include soil fauna in ecosystem and biogeochemical cycle models have largely remained ignored (Grandy et al., 2016; Deckmyn et al., 2020).

Coarse descriptions of soil food webs have been proposed since more than four decades (Coupland, 1979). Among several patterns, the knowledge of biomass distribution among trophic levels can be mobilised into empirical flux models that predict snapshot carbon flows through soil food webs, assuming that the ecosystem is at equilibrium (Gauzens et al., 2019; Jochum et al., 2021). This approach helps identifying the functions of soil communities (Potapov, 2022), and their alteration due to land use for instance (Barnes et al., 2014; Potapov et al., 2019). These studies confirmed the key role of soil fauna in ecosystem functioning (de Vries et al., 2013). Since empirical flux models take biomass distribution among trophic groups as inputs, they cannot predict how environmental changes may modify such distributions and ultimately alter soil functioning. To meet this challenge, designing dynamical models of soil food webs is necessary. The few existing models heading into this direction make use of very simplified food web structure (*e.g.* Huang et al., 2010; Buchkowski et al., 2019; Flores et al., 2021; Buchkowski and Schmitz, 2022) that do not benefit from recent advances in the understanding of soil food web organization (Potapov et al., 2021).

Classical models of food web structure typically assume that trophic levels are correlated with body size (Brose et al., 2006b; Petchey et al., 2008; Quévreux et al., 2021). This assumption suits well to pelagic food webs (Boit et al., 2012; Portalier et al., 2019), but less so to terrestrial food webs in which other traits than body size influence trophic interactions (Valdovinos et al., 2023). Soil food webs in particular are built around multiple energy channels that are based on distinct basal resources, each one being consumed by organisms of various sizes (Wolkovich, 2016). These energy channels are interconnected thanks to many soil organisms that have generalist diets and feed on multiple channels. These soil food web characteristics together blur the correlation between trophic levels and body size (Potapov, 2022). Interestingly, Potapov et al. (2021) proposed a general framework to describe soil food web structure by identifying two sub-food webs: the micro-food web, which is size-structured and relies on microbial production and the macro-food web, which is not size-structured and relies on macro-detritivore production (Fig. 1A). These two sub-food webs are connected by generalist predatory invertebrates such as spiders.

Here, we aim at assessing the ecosystem functioning consequences of this reticulated multichannel structure of soil food webs. To this end, we devised two versions of a dynamic bioenergetic model of soil food web dynamics harbouring either a multichannel structure or a purely size-dependent trophic structure. We parametrised these models with literature data and compared the outputs of the two model versions (*e.g.* biomass distribution, soil respiration and detritus decomposition) to independent worldwide soil ecosystem data. The model-data comparison enabled us to assess the strengths and weaknesses of our models to predict empirical observations, while the comparison of our two model versions enabled us to pinpoint the specific contribution of the multichannel structure of soil food webs to soil ecosystem functioning.

Methods

General description of the model

We developed the Soil MultiChannel Food web (SoMuChFood) model, a bioenergetic food web model based on carbon flows and including six trophic groups and four pools of dead organic matter (Fig. 1A). Here, we provide a brief presentation of the model but a thorough description detailing equations and parameter calculation is available in Appendix S3.

The soil food web is made of six trophic groups: microbes, microbivores and micro-carnivores constituting the micro-food web, and macro-detritivores, macro-carnivores and trophic whales constituting the macro-food web (Fig. 1A). We refer to this first model version including six trophic groups as the multichannel model. We additionally considered a second model version in which macro-detritivores and trophic whales with low trophic levels are neglected, thereby leading to a purely size-structured model in which trophic levels correlate with body size (Fig. 1B).

Each trophic group is separated into trophic species i with different body masses $\overline{M_i}$ spanning over the empirical ranges defined by Potapov et al. (2021) and log uniformly distributed Fig. S3-1 and S2-3 in the supporting information). $\overline{M_i}$ underpins the calculation of biological rates according to allometric relationships drawn from the literature (McCoy and Gillooly, 2008; Johnston and Sibly, 2018; Li et al., 2018, compiled in Tables S2-2 to S2-4 in the supporting information).

We used 10, 4, 9, 12, 15, 9 size classes for microbes, microbivores, micro-carnivores, macro-detritivores, macro-carnivores and trophic whales respectively (to get approximately three size-classes per order of magnitude of body mass range). Modelled consumer dynamics is driven by resource consumption, metabolic losses, predation and non-predation mortality (equation (1a)). Modelled resource dynamics is driven by resource input in the system (for FOM and DOC), resource leaching from the system, resource consumption, resource mortality and resource recycling by consumers for the faeces compartment (equation (1b)).

Predator feeding preferences are size-based, with predators preferring prey 100 times smaller on average (Fig. S2-5 in the supporting information, Brose et al., 2006a), while microbivores and detritivores are not size-restricted. The relative efficiency of microbes and detritivores to consume the various detritus pools depend on their fragmentation. We therefore explicitly represent detritus size and consider that microbes only have access to detritus outer layer (Fig. S2-4 in the supporting information). Consequently, the fragmentation of the FOM induced by its consumption by detritivores favours microbial processing of organic matter by increasing its surface to volume ratio. DOC and SOM can only be consumed by microbes and they are assumed to be fully available for microbes.

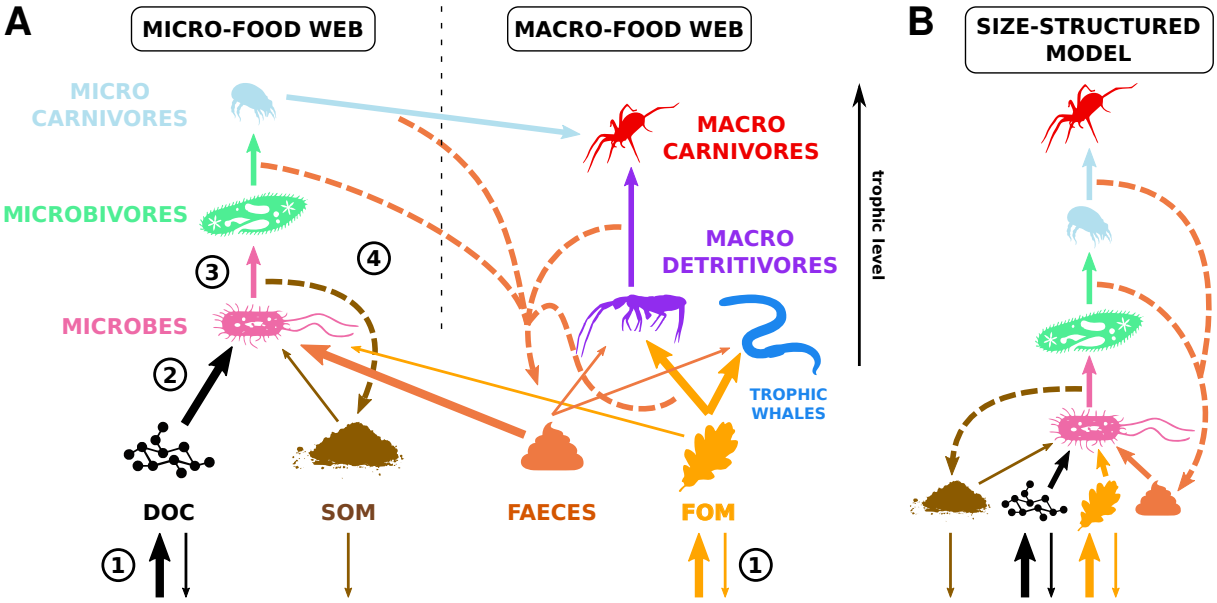

Figure 1: General description of the Soil MultiChannel Food web (SoMuChFood) model. The multichannel version of the model (**A**) contains six trophic groups. Following Potapov et al. (2021), we distinguish microbes, microbivores and micro-carnivores constituting the size structured micro-food web, and macro-detritivores, macro-carnivores and trophic whales constituting the macro-food web. The term "trophic whales" depicts large detritivores that are protected against invertebrate predation. In the size-structured version of the model, macro-detritivores and trophic whales are absent (**B**). Four detritus pools form the abiotic compartment of the ecosystem model in which plant and nutrients such as nitrogen are not explicitly modelled. Dissolved organic carbon (DOC) and fresh organic matter (FOM) represents root exudates and plant litter respectively, and are supplied to the ecosystem by constant external inputs ①. DOC and FOM are lost by leaching while soil organic matter (SOM), which is made of microbial dead materials, is lost by burial in deep soil. Faeces are produced by animals due to inefficient feeding (dashed arrows). Microbes are able to decompose the four detritus types ② but they are more efficient on DOC and faeces, these latter being easily processed by microbes due to the fragmentation of FOM induced by its consumption by detritivores. Predators feed on prey that are smaller in average ③ and generalist macro-carnivores consume both the micro- and the macro-food webs. SOM is made of dead microbes and microbivore faeces, while corpses and faeces other trophic groups contribute to the faeces compartment ④.

Dynamical equations

The general equations of the dynamics of organism's biomass (equation (1a)) and detritus pools (equation (1b)) follow Harfoot et al. (2014) in which the variations of biomass due to each demographic process over a time step Δt are modelled by an exponential function (equation (S2-2) in the supporting information).

$$\Delta B_i(t) = \underbrace{\sum_j^{\text{prey}} \varepsilon_{ij} \Delta B_{ij}(t)}_{\text{resource consumption}} - \underbrace{\sum_j^{\text{pred}} \Delta B_{ji}(t)}_{\text{predation}} - \underbrace{\Delta R_i(t)}_{\text{metabolism}} - \underbrace{\Delta \mu_i(t)}_{\text{mortality}} \tag{1a}$$

$$\Delta B_i(t) = \underbrace{\Delta I}_{\text{input}} - \underbrace{\Delta \ell}_{\text{leaching}} + \underbrace{\sum_k^{\text{species}} \sum_j^{\text{prey}} (1-\varepsilon_{kj}) \Delta B_{kj}(t)}_{\text{nonassimilated biomass}} - \underbrace{\sum_k^{\text{decomposers}} \Delta B_{ki}(t)}_{\text{decomposition}} + \underbrace{\sum_j^{\text{species}} \Delta \mu_j(t)}_{\text{mortality}} \tag{1b}$$

Organisms gain biomass through resource consumption, which is modelled by a Michaelis-Menten functional response for microbes (equation (S2-11)) and a Beddington-DeAngelis functional response for animals (equation (S2-14)). Biomass is lost due to predation, metabolism (respiration) and intrinsic mortality (senescence) defined by allometric relationships, while decomposition parameters are drawn from microbe-based ecosystem models (Wieder et al., 2014). In addition, a fraction of microbial biomass

is able to become dormant if resource uptake is not high enough compared to energy expenditures (Appendix S2-5). Conversely, dormant microbial biomass can be reactivated if resource supply increases. Detritus gain biomass through external inputs (litter fall for the FOM and rhizodeposition for the DOC), inefficient assimilation ($1 - \varepsilon_{ij}$) and mortality. Unassimilated microbial biomass and dead microbes are converted into SOM, unassimilated animal and FOM biomass is converted into faeces and dead animals are converted into FOM (see Fig. S2-1 in the supporting information). FOM, SOM and DOC are also lost by the ecosystem through leaching and burial.

Trophic species are characterised by their trophic level TL_i, which is calculated as the mean of the trophic level of resources weighted by their contribution to consumer's diet, plus one. The trophic level of detritus is set to zero.

$$TL_i = 1 + \frac{\sum_{j}^{prey} \varepsilon_{ij} \Delta B_{ij}(t) TL_j}{\sum_{j}^{prey} \varepsilon_{ij} \Delta B_{ij}(t)} \tag{2}$$

Simulations and parameters

Simulation were run over 4000 days with a time step $\Delta t = 0.01$, which enables the system to reach equilibrium with constant biomass distribution among trophic groups(Fig. S1-11 in the supporting information). We averaged the outputs of the model over the last 100 days of the simulations and considered species as extinct if their biomass falls bellow $1 \times 10^{-10}\,\mathrm{mgC\,m^{-2}}$. The values of the model parameters are reported in Table S2-4 in the supporting information. We performed an extensive sensitivity analysis in Appendix S1-2 to assess the values of some more uncertain parameters.

Empirical data

We compared the outputs of the model with the empirical data compiled by Xu et al. (2013), Johnston and Sibly (2018), and Heděnec et al. (2022) that are available online or on demand. These data sets are representative of the main soil taxa (e.g. nematodes and mites) over the main land biomes of Earth (*e.g.* tropical forest and tundra). We averaged their data over the main biomes and redefined the soil fauna groups to match those defined by Potapov et al. (2021). The estimation of FOM and DOC inputs are based on litter fall (Heděnec et al., 2022) and net primary production (Melillo et al., 1993) data, which is detailed in Appendix S3-9.

Results

Food web structure

As awaited, the two versions of the model predict contrasted relationships between body mass and realised trophic levels, multichannel predictions being better aligned with empirical observations. Indeed, the size-structured model displays a continuous increase in trophic level with body size (Fig. 2A). In contrast, the multichannel model predicts an increase in average trophic level with body size in the micro-food web and a subsequent decrease with increasing body size in the macro-food web (Fig. 2A). The same pattern was empirically observed by Potapov et al. (2021). The hump-shaped relationship between average trophic level and body size has two main drivers. First, the decrease of average trophic level for largest body sizes coincides with the transition between the micro- and the macro-food webs, which is marked by the appearance of detritivorous macro-invertebrates with a low trophic level (purple points in Fig. 2A). Second, there is also a decrease with body mass of average trophic level among the macro-carnivore group, with a lower trophic level of the large macro-carnivores (dark red points) compared to the small ones (light red points). This decrease is due to a diet shift of the macro-carnivores with increasing body size, from feeding mainly on micro-carnivores for smaller species to feeding mainly on macro-detritivores for larger ones (Fig. 2B).

Prediction of biomass distribution

The two model versions predict similar absolute biomasses of the four trophic groups that are present in both model versions (Fig. 3A). The multichannel version additionally predicts a large biomass of macro-detritivores and trophic whales (Fig. 3A). Microbes represent the largest part of the biomass totalling

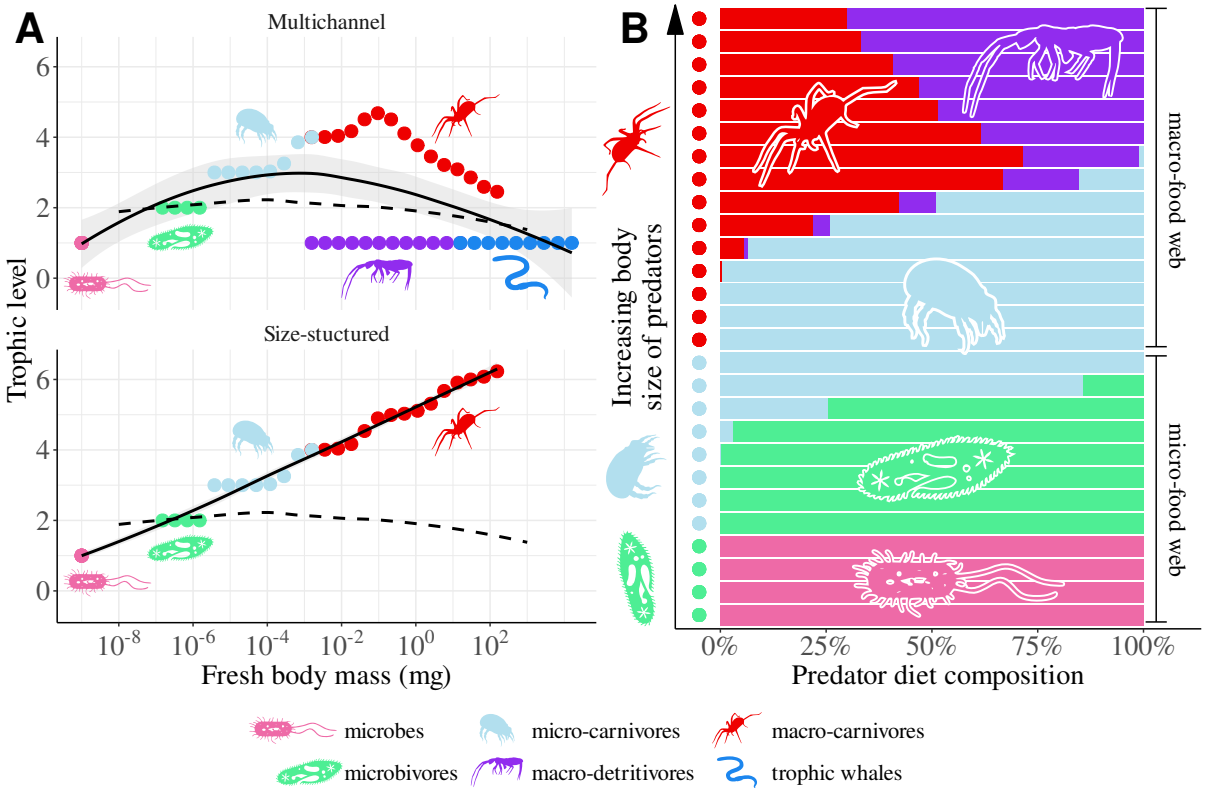

Figure 2: Emerging trophic levels and diets in the two models. **A)** Distribution of trophic levels depending on species fresh body mass for the two food web structures. Dots represent the trophic species (*i.e.* size classes) of each trophic group. The trophic levels TL_i of species i is calculated as the weighted mean of the trophic levels of resources plus one (equation (2)). Solid lines represent the average trophic level, the grey area the standard error and the dashed line the mean trophic level measured in boreal forests by Potapov et al. (2021). The trophic level of resources is set to 0 and decomposers to 1. **B)** Proportion of each trophic group in the diet of predators in the multichannel model.

91% of the biomass in the size-structured model, and 56.3% in the multichannel model (Fig. 3C). The rest of the food web harbours an inverted pyramid biomass distribution, with macro-carnivores accumulating most of the biomass, followed by micro-carnivores and microbivores (Fig. 3A). Quantitatively, these four trophic groups have similar biomass in the two model versions, the macro-carnivores having a slightly larger biomass in the multichannel version, due to their feeding on the additional macro-detritivore group. Interestingly, the size-structured predictions of overall biomass distributions are more aligned with empirical data with microbes representing more than 90% of the total biomass (Fig. 3C) despite being wrong by construction when zooming in the macro-food web due to the absence of detritivorous macro-invertebrates (Fig. 3B). This result is due to the low biomass of the macro-food web compared to the microbial pool in empirical observations (Fig. 3C), contrary to the predictions of the multichannel model in which macro-detritivores and trophic whales are the most abundant animals totalling 34.6% of the soil biomass. Finally, although the multichannel model tends to overestimate the relative contribution of macro-detritivores and trophic whales to the total biomass, it predicts well their predominance in soil fauna biomass (*i.e.* microbes excluded), in agreement with the empirical findings of worldwide syntheses on this topic (Hedĕnec et al., 2022, Fig. 3B).

The predictions of the multichannel model are sensitive to carbon inputs in the system. Very low dissolved organic carbon (DOC) inputs can lead to the collapse of the micro-food web, while very low fresh organic matter (FOM) input can lead to the collapse of the macro-food web (Fig. S1-8 in the supporting information). In contrast, the predictions of the size-structured model are little sensitive to these DOC and FOM input values: the macro-food web always represents a few percent of the total biomass in this model version (Fig. S1-9 in the supporting information). Indeed, the long food chain length in the size-structured model produces an inefficient energy transfer from microbes to macro-carnivores (Fig. 2A). Using input values for dissolved organic carbon and fresh organic matter representative of the major terrestrial biomes, we were able to predict the biomass distribution among trophic groups across biomes. The multichannel model predicts an increasing microbial biomass proportion to the detriment of trophic whales when going from warm to cold biomes, as empirically observed (Fig. 4). It also predicts

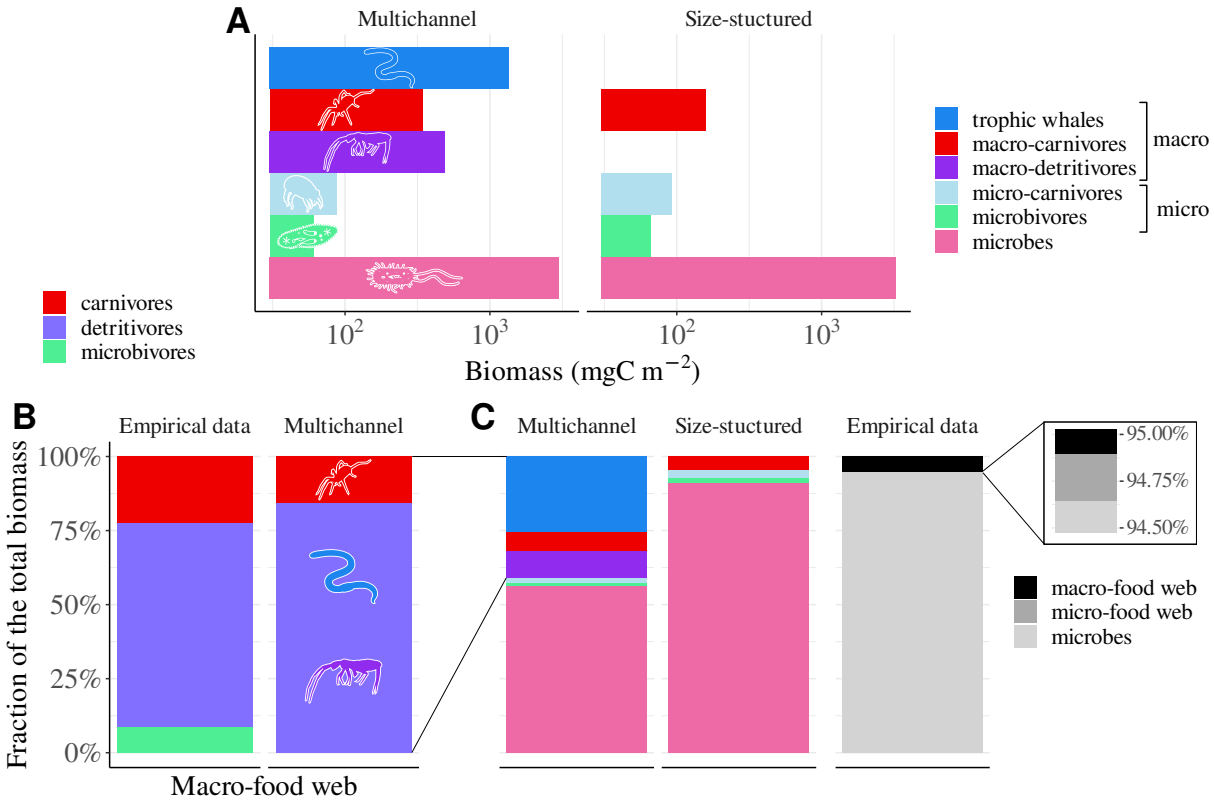

Figure 3: Predicted and observed biomass distribution among trophic groups. **A)** Biomass distribution in the two models. The size-structured model corresponds to the multichannel model without macro-detritivores and trophic whales. **B)** Relative distribution of the biomass among microbivores, detritivores (macro-detritivores + trophic whales) and carnivores in the macro-food webs according to empirical data summarised by Heděnec et al. (2022) and simulations of the multichannel model. **C)** Relative biomass distribution predicted by the two food web models and empirically estimated by Johnston and Sibly (2018) for the sub-food webs. Data across biomes have been pooled (see Fig. S1-10A and B in the supporting information) and the exact percentage values are in Tables S1-1 and S1-2 in the supporting information.

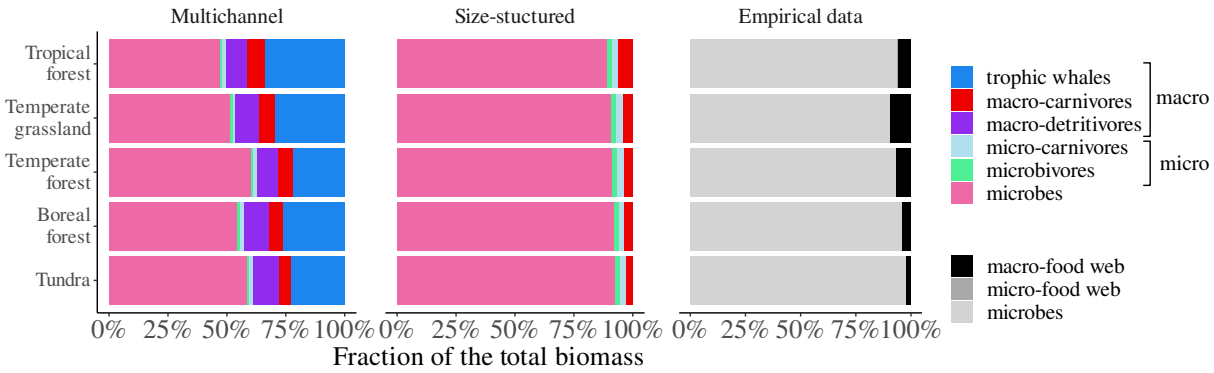

Figure 4: Relative biomass distribution predicted by the two food web models and estimated by Johnston and Sibly (2018) for the major terrestrial biomes. The values of FOM and DOC inputs representative of the considered biomes and used to parametrise the two are summarised in Tables S3-11 and S3-12.

that these inter-biome variations in biomass distributions among trophic groups are of a relatively low magnitude and that a general soil biomass distribution emerges, which is similar to the one reported in Fig. 3B.

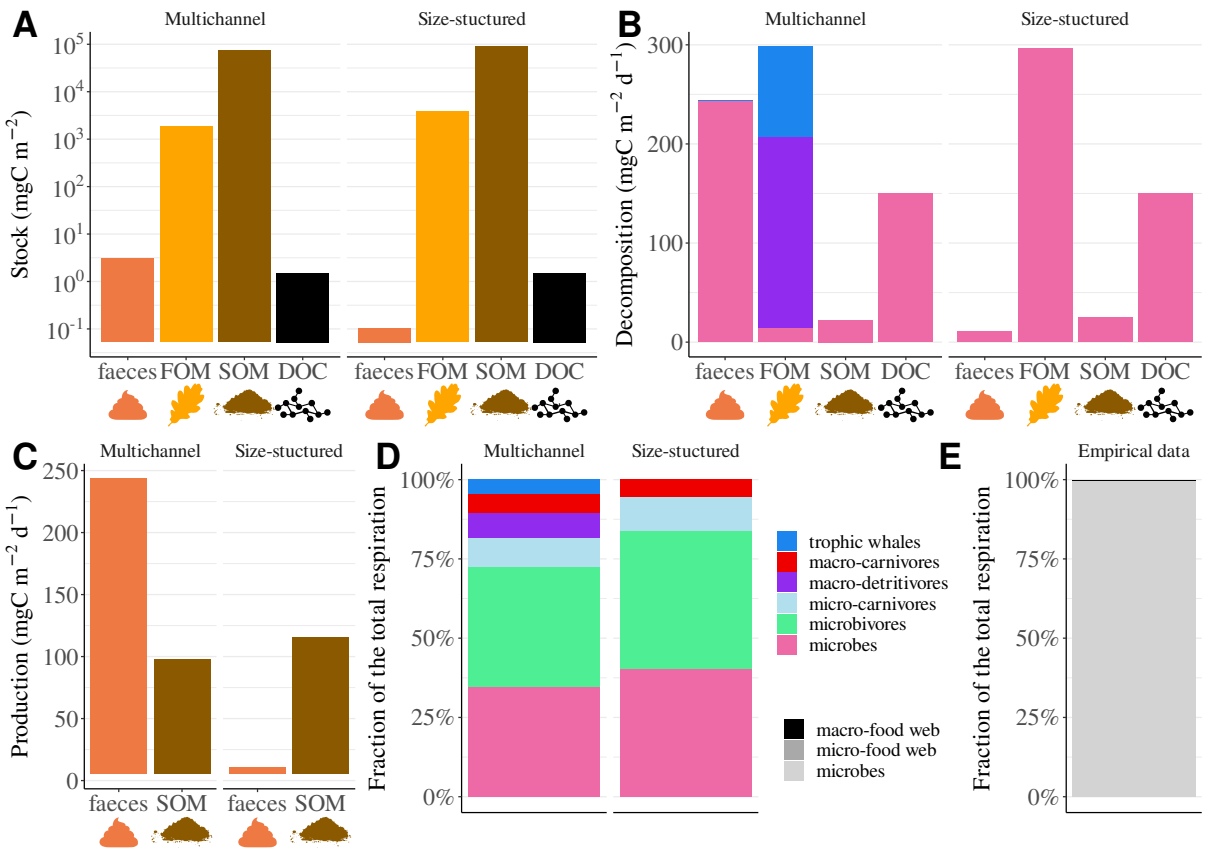

Figure 5: Stocks and fluxes of the various soil carbon pools in the multichannel and size-structured models. **A)** Detritus stocks. **B)** Decomposition rate performed by each decomposer trophic group . **C)** Production rate of each type of detritus by organisms. **D)** Relative distribution of respiration in the multi-channel model. **E)** respiration among the sub-food webs estimated by Johnston and Sibly (2018). Data across biomes have been pooled (see Fig. S1-10A and B in the supporting information) and the exact percentage values are in Tables S1-1 and S1-2 in the supporting information.

Ecosystem functioning

The two models make relatively similar predictions in terms of ecosystem functioning, especially in terms of ecosystem respiration. In both models, soil organic matter (SOM) is the most abundant carbon pool while dissolved organic carbon (DOC) and faeces are heavily depleted (Fig. 5A). In the multichannel model, macro-detritivores and trophic whales consume the majority of the incoming fresh organic matter (FOM, Fig. 5B) but their low assimilation efficiency leads to a strong production of faeces (Fig. 5C). Subsequently, faeces are actively consumed by microbes due to their smaller fragment size and associated larger surface to volume ratio compared to FOM (Fig. 5B). SOM decomposition is very low compared to the one of other detritus pools. This is due to SOM recalcitrance, which enables it to accumulate and to represent the majority of the organic carbon in soils as observed empirically (Table 1a). The two models predict different stocks of detritus: the presence of detritivores in the multichannel model halves the stock of FOM and increases the stock of faeces compared to the size-structured model (Fig. 5A and Table 1b). Microbes are more abundant in the size-structured model because of their consumption of FOM in the place of detritivores (Fig. 5B), which leads to an increase in the stock of SOM (Fig. 5A and Table 1b). Multichannel predictions of the relative pool sizes of FOM and SOM are better aligned with empirical observations (Table 1a) and the attribution of most of the FOM consumption to macro-detritivores is consistent with the findings of numerous macrofauna exclusion experiments that led to a decrease of 14% in FOM decomposition in wet climates (Wall et al., 2008). Both models predict similar (very low) DOC stocks because of their active consumption by microbes. The much lower SOM production compared to faeces/FOM inputs (Fig. 5C) indicates that most of the carbon processed by microbes is lost through metabolism and not stored in the soil, which is confirmed by the strong contribution of microbes to the total respiration in both models (34.7% and 40.2% respectively, Fig. 5D). Finally, both models predict a high contribution of microbivores to the total respiration (37.8% and 43.7% respectively), which strikingly contrasts with model-based estimations that attribute soil respiration nearly entirely to microbes (99.6%, Johnston and Sibly, 2018, Fig. 5E).

Table 1: Comparison of carbon distribution among detrital and microbial pools in the two models and empirical data. Empirical data on FOM are taken from Hedĕnec et al. (2022) and data on SOM and microbial biomass from Xu et al. (2013).

	$C_{mic}/C_{mic+SOM}$	$C_{FOM}/C_{FOM+SOM}$
Multichannel	3.9%	2.4%
Size-structured	3.5%	4.1%
Empirical data	1.2%	2.1%

(a) Ratios between the different pools of carbon C. C_{mic} is the stock of microbial carbon.

Microbial biomass	Faeces	FOM	SOM	DOC
0.92	29.1	0.49	0.83	1

(b) Ratio of the stock values in the multichannel model to the size-structured model.

Discussion

Mechanistic modelling of soil food webs: do the numbers add up?

We developed mechanistic models of soil food webs based on bioenergetic principles and allometric relationships. We calibrated these models with literature data and compared the emerging simulation outputs to independent empirical worldwide data on soil food webs and ecosystem functioning. Modelled food webs with a multichannel structure had realistic trophic properties with a peak of trophic levels for organisms with intermediate body masses (Fig. 2A, Potapov et al., 2021). The multichannel model also compared well with empirical data of biomass distribution among trophic groups with microbial biomass accumulating the major part of the soil biomass (Fig. 3A and C, Johnston and Sibly, 2018), detritivore species accumulating most of the biomass in the macro-food web (Fig. 3A and B, Hedĕnec et al., 2022), and large invertebrates being more abundant than the small ones due to their lower biomass turnover (Ehnes et al., 2014; Ulrich et al., 2015; Potapov et al., 2021). In particular, the multichannel model reproduces well the increasing proportion of microbes in cold biomes characterised by low FOM and DOC inputs (Fig. S1-8 and 4). However, the biomass contribution of the macro-food web to soil biomass predicted by the multichannel model was found to be larger than empirically observed (Fig. 2D). This discrepancy might have several explanations. First, although we were able to collate literature data to parametrise our models, this calibration should be seen as provisional. Indeed, data were scarce for a number of processes that would require additional studies, notably the decomposition of the detritus pools by microbes (see Appendices S1-2 and S3-7). Second, we modelled a single bacteria-like type of microbes with a high biomass turnover, while fungi are known for having a lower biomass turnover and sequester a large amount of carbon (Bailey et al., 2002; Wang et al., 2019). Distinguishing these two groups in our models may thus increase predicted microbial biomass. Third, we modelled the soil invertebrate food web as an isolated system with external carbon inputs (DOC and FOM). By doing so, we neglected additional regulations by vertebrate consumers of soil invertebrates, like birds or burrowing mammals that especially consume soil macro-invertebrates and may therefore decrease their abundances (Scheu, 2001). Finally, we modelled the soil food web as a well-mixed system in which resources are always accessible to their consumers, while soils present a heterogeneous structure with a large variability in pore sizes (Flores et al., 2021). Small pores are likely to constitute refuges for small organisms by being inaccessible to their larger consumers (Deckmyn et al., 2020; Erktan et al., 2020), which may decrease microbial consumption to some extent and thereby increase their relative abundance. Future model improvements along these directions correspond to current research frontiers on the use of functional traits in food web modelling (Brose, 2020, May), on the coupling of above and below-ground food webs (Valdovinos et al., 2023) and on the influence of soil physical structure on trophic interactions (Erktan et al., 2020).

Implications of the multichannel structure for soil ecosystem functioning

Our study further demonstrated that our general soil models predicted realistic carbon stocks and fluxes in and out of the different pools (Fig. 5). The accumulation of microbial biomass is allowed by the dormancy of microbes that offsets the high turnover of their biomass (Fig. S1-6 in the supporting information). The model predicts that only 3.2% (resp. 3.3%) of microbes are active in the multichannel

(resp. size-structured) model, which is consistent with the lower bound reported in the literature (Wang et al., 2014). Interestingly, our results suggest that the multichannel structure of soil food webs, as currently implemented in the SoMuChFood model, has moderate influence on some major features of soil ecosystem functioning such as soil ecosystem respiration and SOM production, since the size-structured version makes similar predictions regarding these features (Fig. 5C and D). The major discrepancy between the two model versions concerns the consumption of fresh organic matter (FOM) that is either operated by macro-detritivores in the multichannel model or directly by microbes in the size-structured model (Fig. 5B). This FOM consumption by macro-detritivores in the multichannel model enables to understand empirical decreases of 14% in litter decomposition in wet climates when excluding macro-organisms reported by the meta-analysis of Wall et al. (2008). Hence, neglecting the multichannel structure of soil food webs may not be problematic for overall predictions of soil ecosystem functioning in undisturbed settings, while adding this refinement may be pivotal to understand the consequences of anthropogenic disturbances on soil ecosystem functioning.

An overlooked role of microbivores in soil functioning?

Our results in both model versions suggest that microbivores (*e.g.* protists) strongly contribute to soil respiration, totalling up to 37.8% of this respiration (Fig. 5D). This sharply contrasts with empirical estimates. For instance, Johnston and Sibly (2018) estimated that microbes contribute more than 99% of soil respiration based on empirical data (Fig. 5E), but these previous estimations were not solely based on direct respiration measurements and were actually also model-based. Indeed, empirical respiration estimates have been conducted at the level of taxonomic groups (*e.g.* microbes, nematodes and termites) based on the biomass of each group and on estimates of mean respiration per individual for each group. We suggest that such previous estimates may present some methodological bias and need a reevaluation. First individual respiration rates have been estimated for the average body size of each group (see Appendix S3-4 for the detailed method), while body sizes of micro-fauna, notably protists, extend over several orders of magnitude (S3-2B in the supporting information). This estimation procedure based on average body sizes may thus underestimate the contribution of micro-fauna to soil respiration since small bodied organisms have a high mass specific metabolic rate. Second, microbial respiration may have been overestimated in this previous study since this model-based approach did not take into account microbial dormancy (Wang et al., 2014). Taken together, these points suggest a more balanced distribution of the total soil respiration between microbes and their predators, which is consistent with the idea that microbivores strongly take part in the turnover of microbial biomass and increase the release of the nutrients immobilised by microbes (de Ruiter et al., 1994; Geisen, 2016; Trap et al., 2016). This suggested balanced distribution of soil respiration between microbes and microbivores may have important consequences when predicting the effects of global changes on soil respiration, and possibly other ecosystem functioning features. For instance, human-induced soil disturbances such as tillage or pesticides decrease the abundance of nematodes (Puissant et al., 2021) and agricultural practices shape protist communities, which drive the top-down control of microbes (Xue et al., 2023) and alter the decomposition of the litter (Geisen et al., 2021). Because they enhance the biomass turnover of microbes and the decomposition of organic matter, microbivores ultimately alter soil respiration patterns in ways difficult to predict without a food web perspective as the one proposed here.

Conclusion

This study demonstrates that a mechanistic understanding of soil food web dynamics is at reach. Although some quantitative mismatch between our model predictions and empirical data do exist, these mismatches pinpoint promising directions for model and experiment improvements. Within ongoing developments of soil ecosystem models, our study focused on assessing the ecosystem functioning consequences of the soil food web multichannel structure. Surprisingly, we found moderate influence of this structure on the main ecosystem functioning features assessed, notably ecosystem respiration and soil organic matter production. Still, the decomposition pathway arising from this multichannel structure is likely to strongly influence soil functioning in disturbed conditions affecting macro-detritivores. Finally, our study suggests that the role of microbivores in soil respiration might have been severely underestimated, with potentially important implications for soil respiration under global changes.

Acknowledgement

We thank Pierre Ganault, François-Xavier Joly, David Ott, Alice Johnston and Jan Frouz for sharing their data and communicating on their methods. We also thank Anton Potapov for the enlighting

discussions on soil food webs, and Julien Pottier and Sébastien Fontaine for their comments on a previous version of the manuscript. This work was funded by the ANR-20-CE32-0004 Astec project, by Campus France through the PHC PROCOPE project number 49348UL and by the French government IDEX-ISITE initiative 16-IDEX-0001 (CAP 20-25).

Data accessibility

The empirical data used in the figures are available online according to associated articles (see Appendix S3) except for Fig. 3D that required data communicated by Jan Frouz. The *R* code to run the simulations, to calculate the parameters and to plot the figures is available on GitHub at the following link: https://github.com/PierreQuevreux/model_SoMuChFood.

References

Bailey, V., Smith, J., & Bolton, H. (2002). Fungal-to-bacterial ratios in soils investigated for enhanced C sequestration. *Soil Biology and Biochemistry*, *34*(7), 997–1007. https://doi.org/10.1016/S0038-0717(02)00033-0

Barnes, A. D., Jochum, M., Mumme, S., Haneda, N. F., Farajallah, A., Widarto, T. H., & Brose, U. (2014). Consequences of tropical land use for multitrophic biodiversity and ecosystem functioning. *Nature Communications*, *5*(1), 5351. https://doi.org/10.1038/ncomms6351

Boit, A., Martinez, N. D., Williams, R. J., & Gaedke, U. (2012). Mechanistic theory and modelling of complex food-web dynamics in Lake Constance. *Ecology Letters*, *15*(6), 594–602. https://doi.org/10.1111/j.1461-0248.2012.01777.x

Brose, U. (2020, May). Trait-based models of complex ecological networks. In *Theoretical Ecology* (pp. 134–142). Oxford University Press. https://doi.org/10.1093/oso/9780198824282.003.0009

Brose, U., Jonsson, T., Berlow, E. L., Warren, P., Banasek-Richter, C., Bersier, L.-F., Blanchard, J. L., Brey, T., Carpenter, S. R., Blandenier, M.-F. C., Cushing, L., Dawah, H. A., Dell, T., Edwards, F., Harper-Smith, S., Jacob, U., Ledger, M. E., Martinez, N. D., Memmott, J., … Cohen, J. E. (2006a). Consumer–resource body-size relationships in natural food webs. *Ecology*, *87*(10), 2411–2417. https://doi.org/10.1890/0012-9658(2006)87[2411:CBRINF]2.0.CO;2

Brose, U., Williams, R. J., & Martinez, N. D. (2006b). Allometric scaling enhances stability in complex food webs. *Ecology Letters*, *9*(11), 1228–1236. https://doi.org/10.1111/j.1461-0248.2006.00978.x

Buchkowski, R. W., Leroux, S. J., & Schmitz, O. J. (2019). Microbial and animal nutrient limitation change the distribution of nitrogen within coupled green and brown food chains [_eprint: https://esajournals.onlinelibrary.wiley.com/doi/pdf/10.1002/ecy.2674]. *Ecology*, *100*(5), e02674. https://doi.org/10.1002/ecy.2674

Buchkowski, R. W., & Schmitz, O. J. (2022). Weak interactions between strong interactors in an old-field ecosystem: Control of nitrogen cycling by coupled herbivores and detritivores. *Functional Ecology*, *36*(1), 133–147. https://doi.org/10.1111/1365-2435.13932

Cebrian, J. (1999). Patterns in the fate of production in plant communities. *The American Naturalist*, *154*(4), 449–468. https://doi.org/10.1086/303244

Coq, S., Ganault, P., Le Mer, G., Nahmani, J., Capowiez, Y., Dignac, M.-F., Rumpel, C., & Joly, F.-X. (2022). Faeces traits as unifying predictors of detritivore effects on organic matter turnover. *Geoderma*, *422*, 115940. https://doi.org/10.1016/j.geoderma.2022.115940

Coupland, R. T. (Ed.). (1979). *Grassland ecosystems of the world: Analysis of grasslands and their uses*. Cambridge University Press.

Crowther, T. W., van den Hoogen, J., Wan, J., Mayes, M. A., Keiser, A. D., Mo, L., Averill, C., & Maynard, D. S. (2019). The global soil community and its influence on biogeochemistry. *Science*, *365*(6455), eaav0550. https://doi.org/10.1126/science.aav0550

Deckmyn, G., Flores, O., Mayer, M., Domene, X., Schnepf, A., Kuka, K., Van Looy, K., Rasse, D. P., Briones, M. J., Barot, S., Berg, M., Vanguelova, E., Ostonen, I., Vereecken, H., Suz, L. M., Frey, B., Frossard, A., Tiunov, A., Frouz, J., … Curiel Yuste, J. (2020). KEYLINK: Towards a more integrative soil representation for inclusion in ecosystem scale models. I. review and model concept. *PeerJ*, *8*, e9750. https://doi.org/10.7717/peerj.9750

de Ruiter, P. C., Neutel, A.-M., & Moore, J. C. (1994). Modelling food webs and nutrient cycling in agro-ecosystems. *Trends in Ecology & Evolution*, *9*(10), 378–383. https://doi.org/10.1016/0169-5347(94)90059-0

de Vries, F. T., Thébault, E., Liiri, M., Birkhofer, K., Tsiafouli, M. A., Bjørnlund, L., Bracht Jørgensen, H., Brady, M. V., Christensen, S., de Ruiter, P. C., d'Hertefeldt, T., Frouz, J., Hedlund, K., Hemerik, L., Hol, W. H. G., Hotes, S., Mortimer, S. R., Setälä, H., Sgardelis, S. P., … Bardgett, R. D. (2013). Soil food web properties explain ecosystem services across European land use systems. *Proceedings of the National Academy of Sciences*, *110*(35), 14296–14301. https://doi.org/10.1073/pnas.1305198110

Ehnes, R. B., Pollierer, M. M., Erdmann, G., Klarner, B., Eitzinger, B., Digel, C., Ott, D., Maraun, M., Scheu, S., & Brose, U. (2014). Lack of energetic equivalence in forest soil invertebrates. *Ecology*, *95*(2), 527–537. https://doi.org/10.1890/13-0620.1

Erktan, A., Or, D., & Scheu, S. (2020). The physical structure of soil: Determinant and consequence of trophic interactions. *Soil Biology and Biochemistry*, *148*, 107876. https://doi.org/10.1016/j.soilbio.2020.107876

Flores, O., Deckmyn, G., Curiel Yuste, J., Javaux, M., Uvarov, A., van der Linde, S., De Vos, B., Vereecken, H., Jiménez, J., Vinduskova, O., & Schnepf, A. (2021). KEYLINK: Towards a more integrative soil representation for inclusion in ecosystem scale models—II: Model description, implementation and testing. *PeerJ*, *9*, e10707. https://doi.org/10.7717/peerj.10707

Gauzens, B., Barnes, A., Giling, D. P., Hines, J., Jochum, M., Lefcheck, J. S., Rosenbaum, B., Wang, S., & Brose, U. (2019). *fluxweb* : An R package to easily estimate energy fluxes in food webs (S. Goslee, Ed.). *Methods in Ecology and Evolution*, *10*(2), 270–279. https://doi.org/10.1111/2041-210X.13109

Geisen, S. (2016). The bacterial-fungal energy channel concept challenged by enormous functional versatility of soil protists. *Soil Biology and Biochemistry*, *102*, 22–25. https://doi.org/10.1016/j.soilbio.2016.06.013

Geisen, S., Hu, S., Dela Cruz, T. E. E., & Veen, G. F. (2021). Protists as catalyzers of microbial litter breakdown and carbon cycling at different temperature regimes. *The ISME Journal*, *15*(2), 618–621. https://doi.org/10.1038/s41396-020-00792-y

Grandy, A. S., Wieder, W. R., Wickings, K., & Kyker-Snowman, E. (2016). Beyond microbes: Are fauna the next frontier in soil biogeochemical models? *Soil Biology and Biochemistry*, *102*, 40–44. https://doi.org/10.1016/j.soilbio.2016.08.008

Harfoot, M. B. J., Newbold, T., Tittensor, D. P., Emmott, S., Hutton, J., Lyutsarev, V., Smith, M. J., Scharlemann, J. P. W., & Purves, D. W. (2014). Emergent global patterns of ecosystem structure and function from a mechanistic general ecosystem model (M. Loreau, Ed.). *PLoS Biology*, *12*(4), e1001841. https://doi.org/10.1371/journal.pbio.1001841

Heděnec, P., Jiménez, J. J., Moradi, J., Domene, X., Hackenberger, D., Barot, S., Frossard, A., Oktaba, L., Filser, J., Kindlmann, P., & Frouz, J. (2022). Global distribution of soil fauna functional groups and their estimated litter consumption across biomes. *Scientific Reports*, *12*(1), 17362. https://doi.org/10.1038/s41598-022-21563-z

Huang, C.-Y., Hendrix, P. F., Fahey, T. J., Bohlen, P. J., & Groffman, P. M. (2010). A simulation model to evaluate the impacts of invasive earthworms on soil carbon dynamics. *Ecological Modelling*, *221*(20), 2447–2457. https://doi.org/10.1016/j.ecolmodel.2010.06.023

Jochum, M., Barnes, A. D., Brose, U., Gauzens, B., Sünnemann, M., Amyntas, A., & Eisenhauer, N. (2021). For flux's sake: General considerations for energy-flux calculations in ecological communities. *Ecology and Evolution*, *11*(19), 12948–12969. https://doi.org/10.1002/ece3.8060

Johnston, A. S. A., & Sibly, R. M. (2018). The influence of soil communities on the temperature sensitivity of soil respiration. *Nature Ecology & Evolution*, *2*(10), 1597–1602. https://doi.org/10.1038/s41559-018-0648-6

Joly, F.-X., Coq, S., Coulis, M., David, J.-F., Hättenschwiler, S., Mueller, C. W., Prater, I., & Subke, J.-A. (2020). Detritivore conversion of litter into faeces accelerates organic matter turnover. *Communications Biology*, *3*(1), 660. https://doi.org/10.1038/s42003-020-01392-4

Li, Y., Rall, B. C., & Kalinkat, G. (2018). Experimental duration and predator satiation levels systematically affect functional response parameters. *Oikos*, *127*(4), 590–598. https://doi.org/10.1111/oik.04479

McCoy, M. W., & Gillooly, J. F. (2008). Predicting natural mortality rates of plants and animals. *Ecology Letters*, *11*(7), 710–716. https://doi.org/10.1111/j.1461-0248.2008.01190.x

Melillo, J. M., McGuire, A. D., Kicklighter, D. W., Moore, B., Vorosmarty, C. J., & Schloss, A. L. (1993). Global climate change and terrestrial net primary production. *Nature*, *363*(6426), 234–240. https://doi.org/10.1038/363234a0

Minasny, B., Malone, B. P., McBratney, A. B., Angers, D. A., Arrouays, D., Chambers, A., Chaplot, V., Chen, Z.-S., Cheng, K., Das, B. S., Field, D. J., Gimona, A., Hedley, C. B., Hong, S. Y., Mandal, B., Marchant, B. P., Martin, M., McConkey, B. G., Mulder, V. L., … Winowiecki, L. (2017). Soil carbon 4 per mille. *Geoderma*, *292*, 59–86. https://doi.org/10.1016/j.geoderma.2017.01.002

Perveen, N., Barot, S., Alvarez, G., Klumpp, K., Martin, R., Rapaport, A., Herfurth, D., Louault, F., & Fontaine, S. (2014). Priming effect and microbial diversity in ecosystem functioning and response to global change: A modeling approach using the SYMPHONY model. *Global Change Biology*, *20*(4), 1174–1190. https://doi.org/10.1111/gcb.12493

Petchey, O. L., Beckerman, A. P., Riede, J. O., & Warren, P. H. (2008). Size, foraging, and food web structure. *Proceedings of the National Academy of Sciences*, *105*(11), 4191–4196. https://doi.org/10.1073/pnas.0710672105

Portalier, S. M. J., Fussmann, G. F., Loreau, M., & Cherif, M. (2019). The mechanics of predator–prey interactions: First principles of physics predict predator–prey size ratios. *Functional Ecology*, *33*(2), 323–334. https://doi.org/10.1111/1365-2435.13254

Potapov, A. M. (2022). Multifunctionality of belowground food webs: Resource, size and spatial energy channels. *Biological Reviews*, *97*(4), 1691–1711. https://doi.org/10.1111/brv.12857

Potapov, A. M., Klarner, B., Sandmann, D., Widyastuti, R., & Scheu, S. (2019). Linking size spectrum, energy flux and trophic multifunctionality in soil food webs of tropical land-use systems (A. Eklöf, Ed.). *Journal of Animal Ecology*, *88*(12), 1845–1859. https://doi.org/10.1111/1365-2656.13027

Potapov, A. M., Rozanova, O. L., Semenina, E. E., Leonov, V. D., Belyakova, O. I., Bogatyreva, V. Y., Degtyarev, M. I., Esaulov, A. S., Korotkevich, A. Y., Kudrin, A. A., Malysheva, E. A., Mazei, Y. A., Tsurikov, S. M., Zuev, A. G., & Tiunov, A. V. (2021). Size compartmentalization of energy channeling in terrestrial belowground food webs. *Ecology*, *102*(8). https://doi.org/10.1002/ecy.3421

Puissant, J., Villenave, C., Chauvin, C., Plassard, C., Blanchart, E., & Trap, J. (2021). Quantification of the global impact of agricultural practices on soil nematodes: A meta-analysis. *Soil Biology and Biochemistry*, *161*, 108383. https://doi.org/10.1016/j.soilbio.2021.108383

Quévreux, P., Barot, S., & Thébault, É. (2021). Interplay between the paradox of enrichment and nutrient cycling in food webs. *Oikos*, *130*(1), 95–109. https://doi.org/10.1111/oik.07937

Scheu, S. (2001). Plants and generalist predators as links between the below-ground and above-ground system. *Basic and Applied Ecology*, *2*(1), 3–13. https://doi.org/10.1078/1439-1791-00031

Trap, J., Bonkowski, M., Plassard, C., Villenave, C., & Blanchart, E. (2016). Ecological importance of soil bacterivores for ecosystem functions. *Plant and Soil*, *398*(1-2), 1–24. https://doi.org/10.1007/s11104-015-2671-6

Ulrich, W., Hoste-Danyłow, A., Faleńczyk-Koziróg, K., Hajdamowicz, I., Ilieva-Makulec, K., Olejniczak, I., Stańska, M., & Wytwer, J. (2015). Temporal patterns of energy equivalence in temperate soil invertebrates. *Oecologia*, *179*(1), 271–280. https://doi.org/10.1007/s00442-015-3317-3

Valdovinos, F. S., Hale, K. R., Dritz, S., Glaum, P. R., McCann, K. S., Simon, S. M., Thébault, E., Wetzel, W. C., Wootton, K. L., & Yeakel, J. D. (2023). A bioenergetic framework for aboveground terrestrial food webs. *Trends in Ecology & Evolution*, *38*(3), 301–312. https://doi.org/10.1016/j.tree.2022.11.004

Wall, D. H., Bradford, M. A., St. John, M. G., Trofymow, J. A., Behan-Pelletier, V., Bignell, D. E., Dangerfield, J. M., Parton, W. J., Rusek, J., Voigt, W., Wolters, V., Gardel, H. Z., Ayuke, F. O., Bashford, R., Beljakova, O. I., Bohlen, P. J., Brauman, A., Flemming, S., Henschel, J. R., … Zou, X. (2008). Global decomposition experiment shows soil animal impacts on decomposition are climate-dependent. *Global Change Biology*, *14*(11), 2661–2677. https://doi.org/10.1111/j.1365-2486.2008.01672.x

Wang, G., Mayes, M. A., Gu, L., & Schadt, C. W. (2014). Representation of dormant and active microbial dynamics for ecosystem modeling (J. H. Badger, Ed.). *PLoS ONE*, *9*(2), e89252. https://doi.org/10.1371/journal.pone.0089252

Wang, X., Zhang, W., Shao, Y., Zhao, J., Zhou, L., Zou, X., & Fu, S. (2019). Fungi to bacteria ratio: Historical misinterpretations and potential implications. *Acta Oecologica*, *95*, 1–11. https://doi.org/10.1016/j.actao.2018.10.003

Wieder, W. R., Grandy, A. S., Kallenbach, C. M., & Bonan, G. B. (2014). Integrating microbial physiology and physio-chemical principles in soils with the MIcrobial-MIneral Carbon Stabilization (MIMICS) model. *Biogeosciences*, *11*(14), 3899–3917. https://doi.org/10.5194/bg-11-3899-2014

Wieder, W. R., Bonan, G. B., & Allison, S. D. (2013). Global soil carbon projections are improved by modelling microbial processes. *Nature Climate Change*, *3*(10), 909–912. https://doi.org/10.1038/nclimate1951

Wolkovich, E. M. (2016). Reticulated channels in soil food webs. *Soil Biology and Biochemistry*, *102*, 18–21. https://doi.org/10.1016/j.soilbio.2016.06.021

Xu, X., Thornton, P. E., & Post, W. M. (2013). A global analysis of soil microbial biomass carbon, nitrogen and phosphorus in terrestrial ecosystems: Global soil microbial biomass C, N and P. *Global Ecology and Biogeography*, *22*(6), 737–749. https://doi.org/10.1111/geb.12029

Xue, P., Minasny, B., McBratney, A., Jiang, Y., & Luo, Y. (2023). Land use effects on soil protists and their top-down regulation on bacteria and fungi in soil profiles. *Applied Soil Ecology*, *185*, 104799. https://doi.org/10.1016/j.apsoil.2022.104799

S1 Complementary results

S1-1 Detailed results

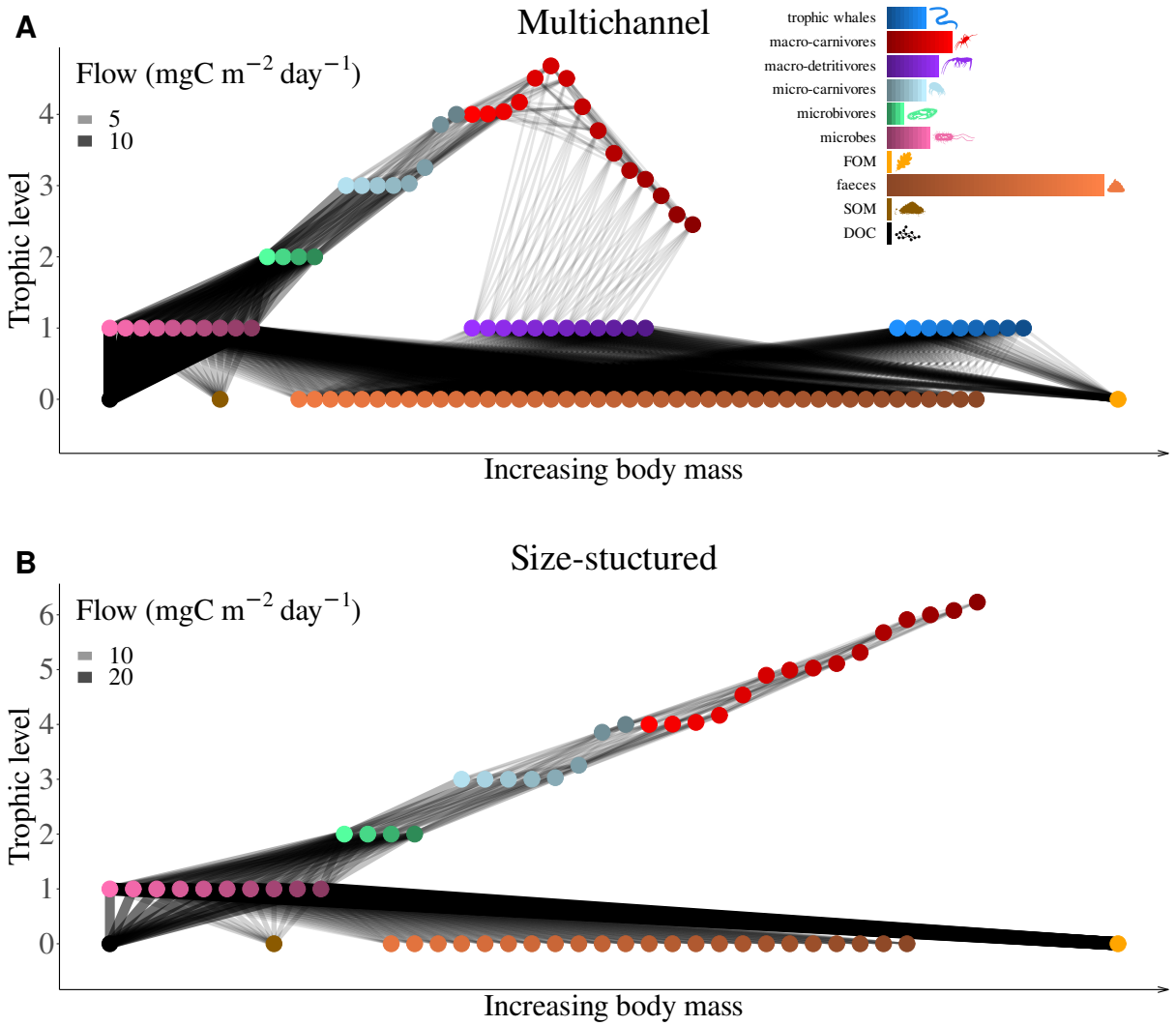

Figure S1-1: Graphical representation of the food web structure according to trophic levels and body size. Trophic level 0 represents the detritus pools. **A)** Multichannel model. **B)** Size structured model.

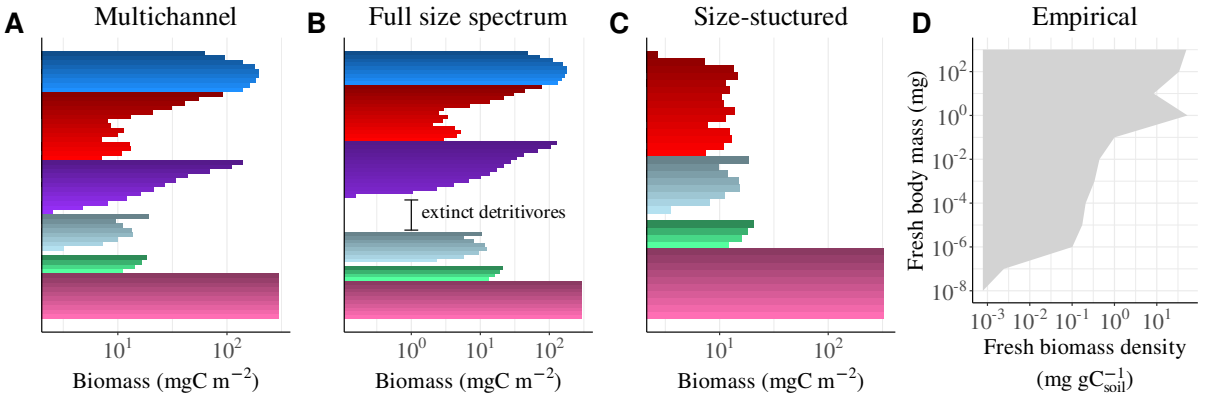

Figure S1-2: Distribution of the biomass among species (*i.e.* size classes, see Fig. S2-3) in the three food web models (see Fig. S3-1). **A)** Multichannel model (main model). **B)** Full size spectrum containing micro-detritivores. **C)** Size-structured model without macro-detritivores and trophic whales (null model). **D)** Abundance of organisms depending on their body mass measured by Potapov et al. (2021).

Table S1-1: Distribution of the biomass in the two food web models.

Trophic group	Multichannel biomass Fig. 3B	Size-structured biomass Fig. 3B	Multichannel respiration Fig. 3C	Size-structured respiration Fig. 3C
Microbes	56.3%	91%	34.7%	40.2%
Microbivores	1.1%	1.9%	37.8%	43.7%
Micro-carnivores	1.6%	2.6%	9.3%	10.6%
Macro-detritivores	9.2%	-	7.9%	-
Macro-carnivores	6.4%	4.5%	5.9%	5.5%
Trophic whales	25.4%	-	4.4%	-

Trophic group	Multichannel active biomass Fig. S1-6B	Size-structured active biomass Fig. S1-6B
Microbes	3.9%	24.9%
Microbivores	2.5%	15.7%
Micro-carnivores	3.6%	21.9%
Macro-detritivores	20.2%	-
Macro-carnivores	14.1%	37.5%
Trophic whales	55.7%	-

Table S1-2: Distribution of the biomass and of the respiration according to Johnston and Sibly (2018).

	Biomass Fig. 3B	Respiration Fig. 3B
Microbes	94.6%	99.6%
Micro-food web	0.3%	0.1%
Macro-food web	5.1%	0.3%

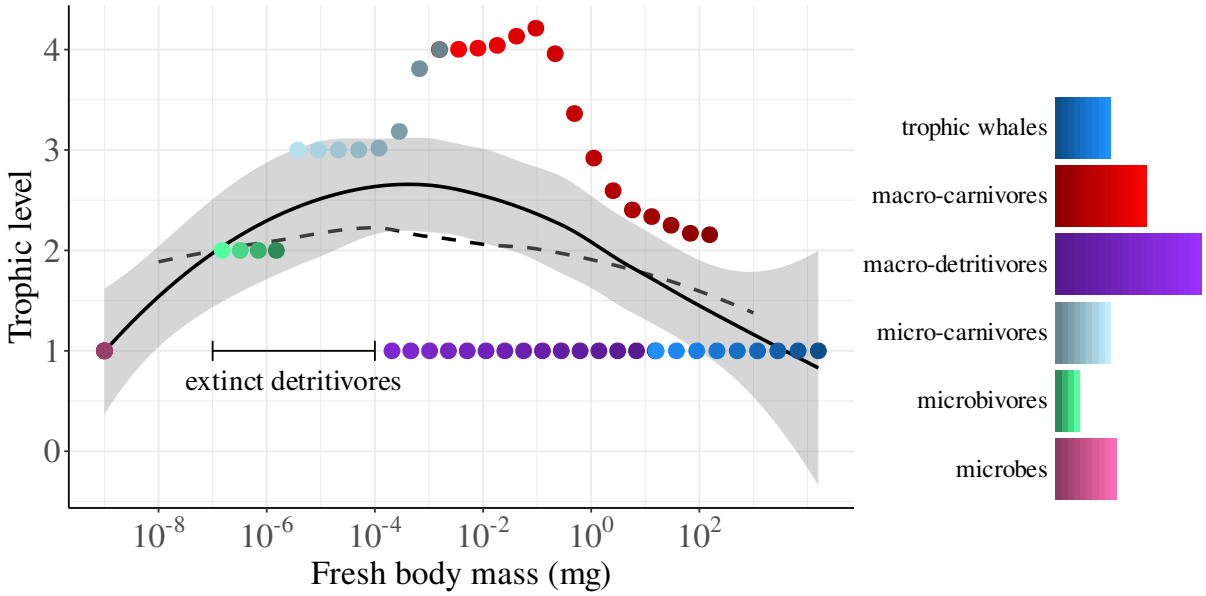

Figure S1-3: Distribution of trophic levels in the full detritivore body mass spectrum model (see Fig. S3-1). Solid lines represent the average trophic level, the grey area the standard error and the dashed line the mean trophic level measured in boreal forests by Potapov et al. (2021). The trophic level of resources is set to 0 and decomposers to 1.

The key feature of the multichannel model compared to the size-structured model is the presence of large bodied detritivores that break the linear relation between body size and trophic levels (Fig. 2A).

Interestingly, the absence of small sized invertebrate decomposers is predicted by our model: in additional simulations in which we considered "micro-detritivores" (Fig. S3-1 in the supporting information), they got extinct because of the apparent competition with microbes mediated by micro-carnivores (Fig. S1-2 and S1-3 in the supporting information). This absence can also be explained by the requirement of particular traits that enable detritivores to shred into pieces and to consume the FOM (Pollierer et al., 2007; Potapov et al., 2022), traits only present for large bodied invertebrates.

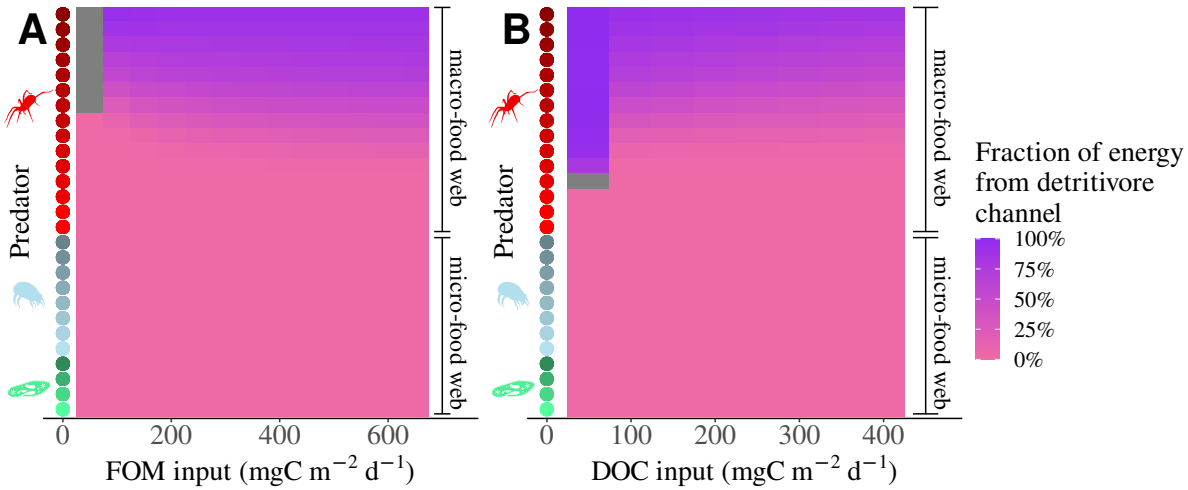

Figure S1-4: Fraction of the energy consumed by each predator in the multichannel model driven from the detritivore channel depending on the **A)** FOM input (DOC input equal to 150 mgC m^{-2} d^{-1}) or **B)** DOC input (FOM input equal to 300 mgC m^{-2} d^{-1}). The other fraction represents the energy driven from the microbial channel. The fraction of energy from the detritivore channel X_i obtained by species i is calculated as the mean of the fraction of energy X_j of resources weighted by their contribution to consumer's diet $\varepsilon_{ij}\Delta B_{ij}$. X_i is set to 1 for detritivores and 0 for microbes.

$$X_i = \frac{\sum_{j}^{prey} \varepsilon_{ij}\Delta B_{ij}(t) X_j}{\sum_{j}^{prey} \varepsilon_{ij}\Delta B_{ij}(t)}$$

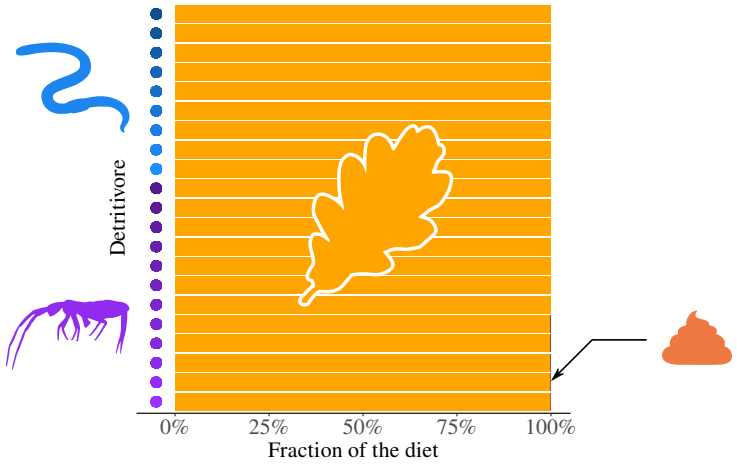

Figure S1-5: Diet of invertebrate detritivores in the multichannel model. They quasi exclusively feed on FOM. They do not eat on microbes while feeding on detritus because most of the microbes live on the SOM which has a a much higher surface to volume ratio.

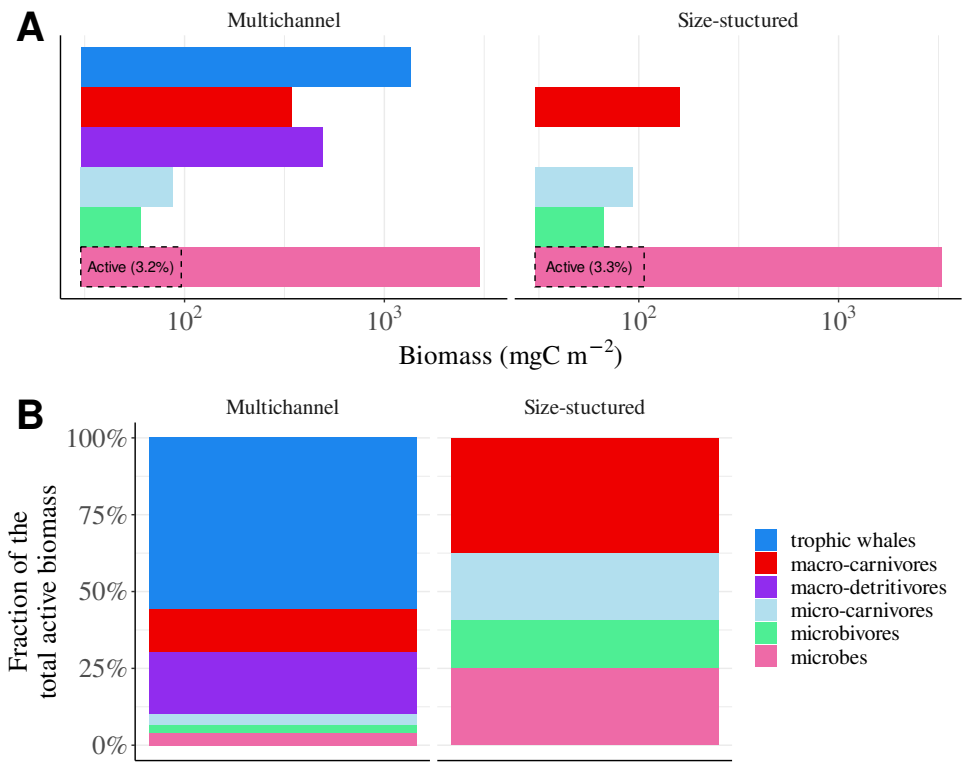

Figure S1-6: Importance of microbial activity in the multichannel model. **A)** Distribution of biomass among species. The dashed rectangle represents the fraction of active microbes. **B)** Relative contribution of each trophic group to the total biomass in which only the fraction of active microbes is represented.

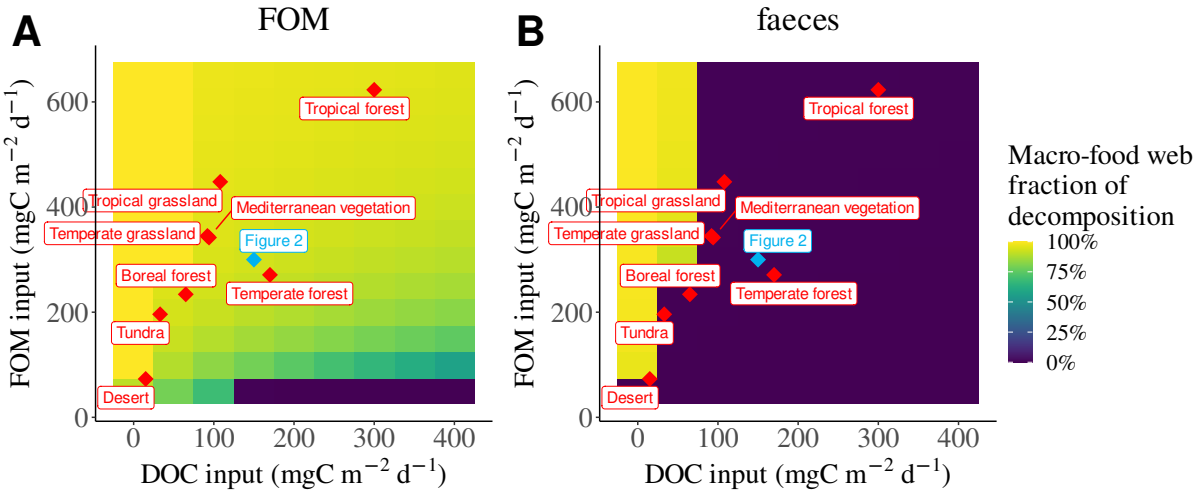

Figure S1-7: Contribution of macro-detritivores to detritus decomposition relative to the total contribution of all decomposers. Decomposition is calculated for different inputs of FOM and SOM and the red diamonds correspond to the estimated inputs of various ecosystems. **A)** FOM. **B)** Faeces.

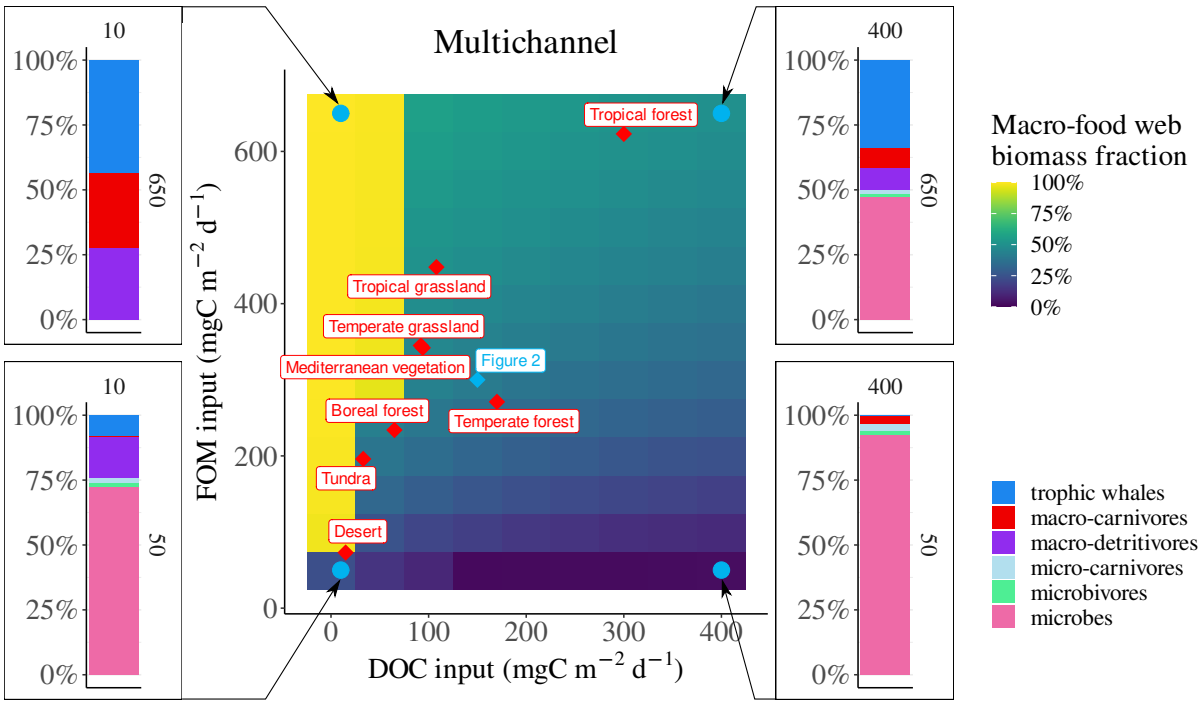

Figure S1-8: Fraction of macro-food web biomass relative to the total biomass for different inputs of FOM and DOC in the multichannel model. The four subplots represent the detailed distribution of the biomass for particular inputs mapped by blue points. The blue diamond depicts the inputs considered in Fig. 3 (reported in Table S2-3 in the supporting information) and the red diamonds correspond to the estimated inputs for various biomes whose corresponding FOM and DOC inputs are summarised in Tables S3-11 and S3-12.

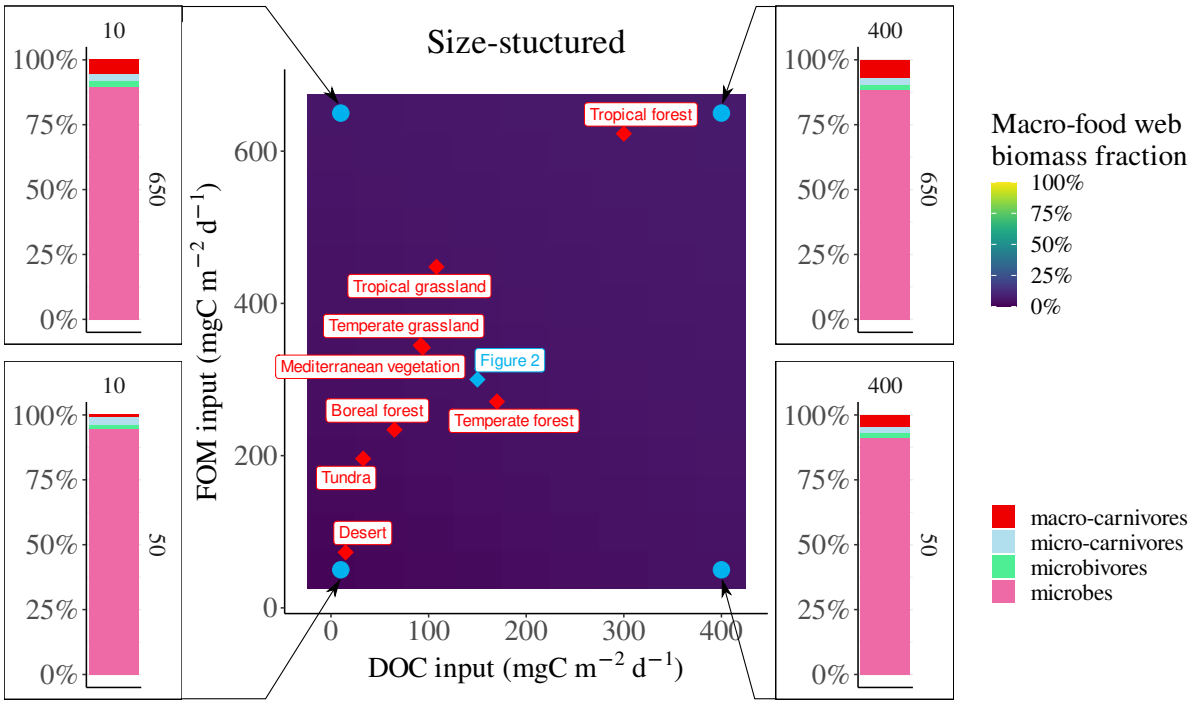

Figure S1-9: Fraction of macro-food web biomass relative to the total biomass for different inputs of FOM and DOC in the size-structured model. The four subplots represent the detailed distribution of the biomass for particular inputs mapped by blue points. The blue diamond depicts the inputs considered in Fig. 3 (reported in Table S2-3 in the supporting information) and the red diamonds correspond to the estimated inputs for various biomes whose corresponding FOM and DOC inputs are summarised in Tables S3-11 and S3-12.

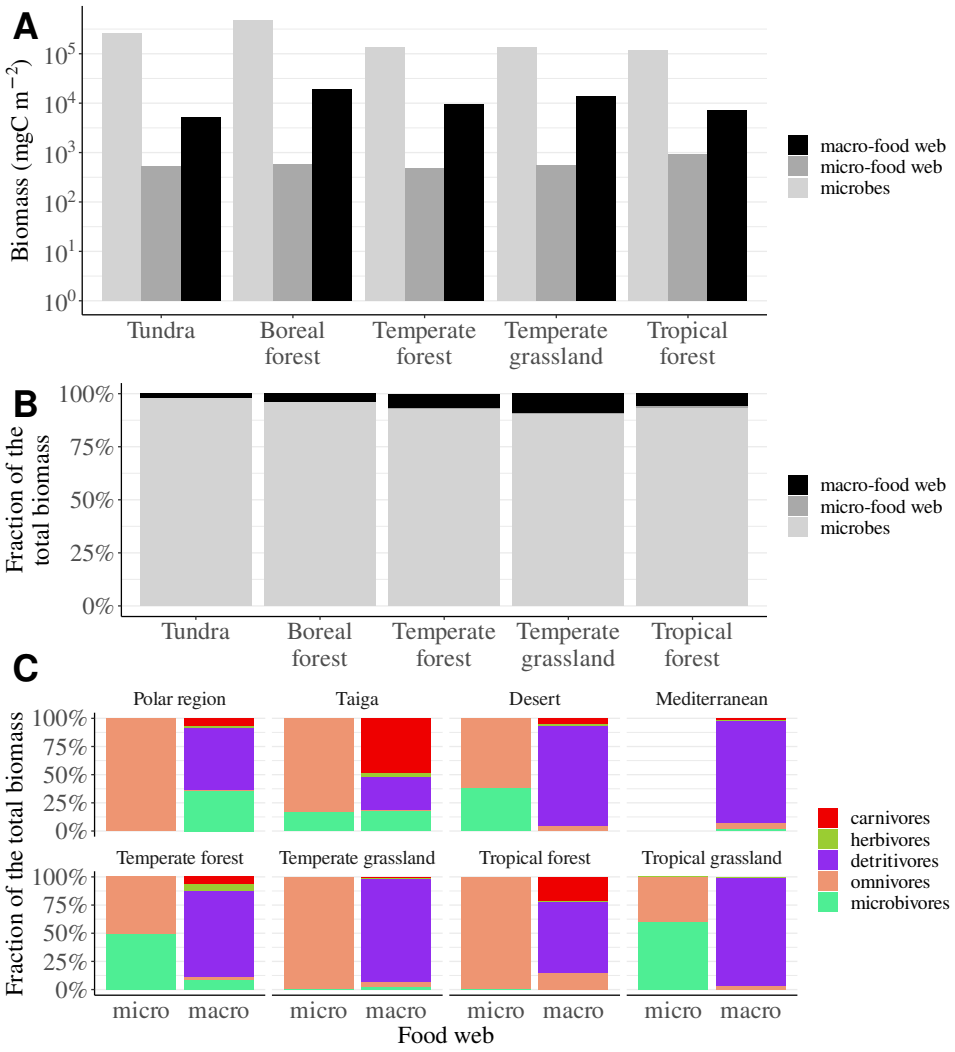

Figure S1-10: Biomass distribution across biomes. **A)** Average biomass distribution among the three sub-food webs (data from Johnston and Sibly, 2018). **A)** Average relative biomass distribution among the three sub-food webs. **B)** Biomass distribution among the main trophic types in the micro- and macro-food webs (data from Heděnec et al., 2022). In Fig. 3 in the main text, herbivores have been removed and omnivores have been merged with carnivores.

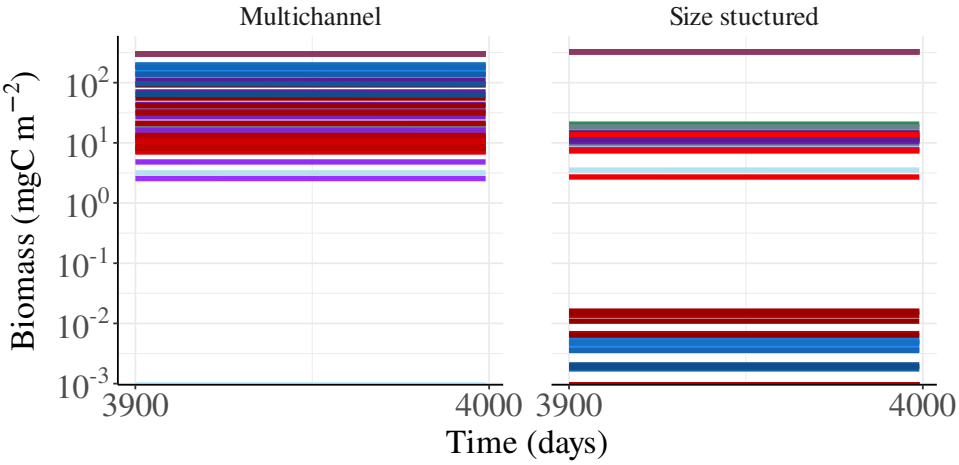

Figure S1-11: Time series of the multichannel and size structured models showing that the system has reached equilibrium.

S1-2 Sensitivity analysis

S1-2-1 Organic matter decomposition half-saturation

The half-saturation K_{Cj} of the decomposition of the detritus pool j by microbes has been assessed according to Grover (2003) and German et al. (2012) (see Appendix S3-7 for more details). However, the values are only estimations and require some adjustment to run the model properly (Wieder et al., 2014). We have crossed three values of the tuning coefficient a_K of the DOC, SOM and FOM-faeces (which share the same uptake function, see equation (S2-12)), found that they do not significantly affect the distribution of species biomass or detritus pools and kept the values $a_{KDOC} = 0.01$, $a_{KFOM} = 0.001$ and $a_{KSOM} = 0.001$

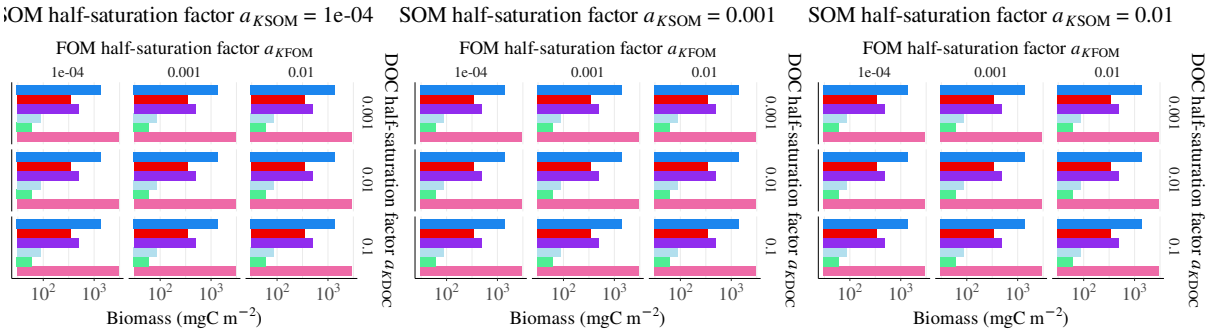

Figure S1-12: Biomass distribution among trophic groups depending on the half-saturation factors of the decomposition of FOM (a_{KFOM}), SOM (a_{KSOM}) and DOC (a_{KDOC}).

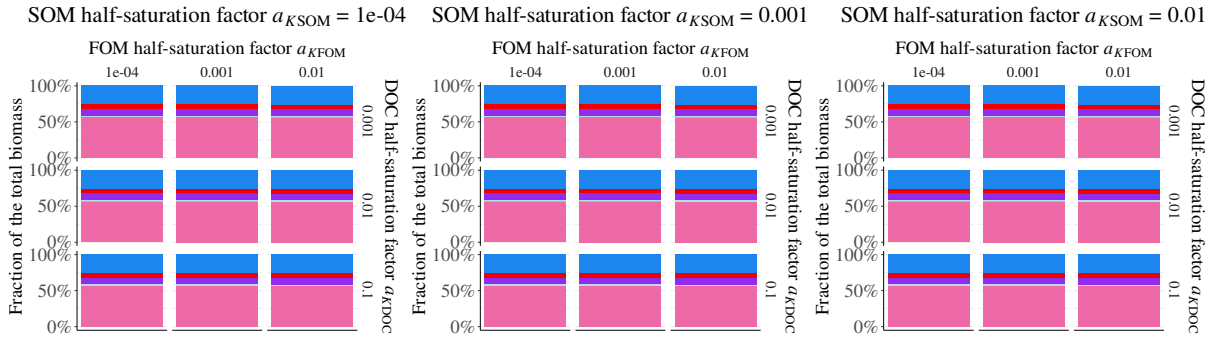

Figure S1-13: Relative biomass distribution depending on the half-saturation factors of the decomposition of FOM (a_{KFOM}), SOM (a_{KSOM}) and DOC (a_{KDOC}).

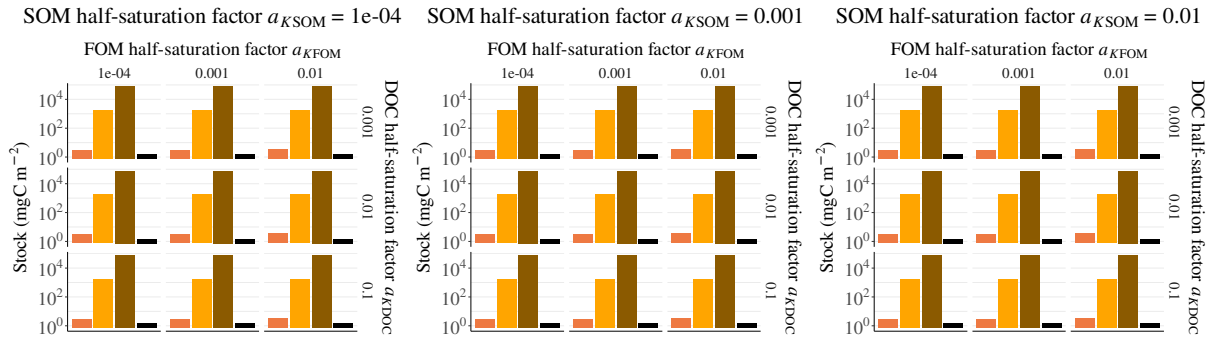

Figure S1-14: Detritus stocks depending on the half-saturation factors of the decomposition of FOM (a_{KFOM}), SOM (a_{KSOM}) and DOC (a_{KDOC}).

S1-2-2 Organic matter decomposition rate

In the same vein, we adjusted the maximum decomposition rate φ_{Cj}^{max} of the various detritus pools j with the tuning parameter a_φ. We keep $a_{\varphi DOC} = 10$, $a_{\varphi FOM} = 1000$ and $a_{\varphi SOM} = 10$ according to the criteria summarised in Table S1-3.

Table S1-3: Distribution of the biomass for the two food web structures.

Criterion	$a_{\varphi DOC}$	$a_{\varphi FOM}$	$a_{\varphi SOM}$	Figure
Species persistence	-	$\geqslant 10$	-	S1-15
Accumulation of SOM and depletion of DOC	-	-	< 100	S1-16
Large fraction of microbes	-	1000	-	S1-17
Decomposition of faeces by microbes	-	1000	-	S1-18
Realistic decomposition rate	-	1000	10	S1-19
Equilibrium	10	-	-	S1-20
Final value	**10**	**1000**	**10**	

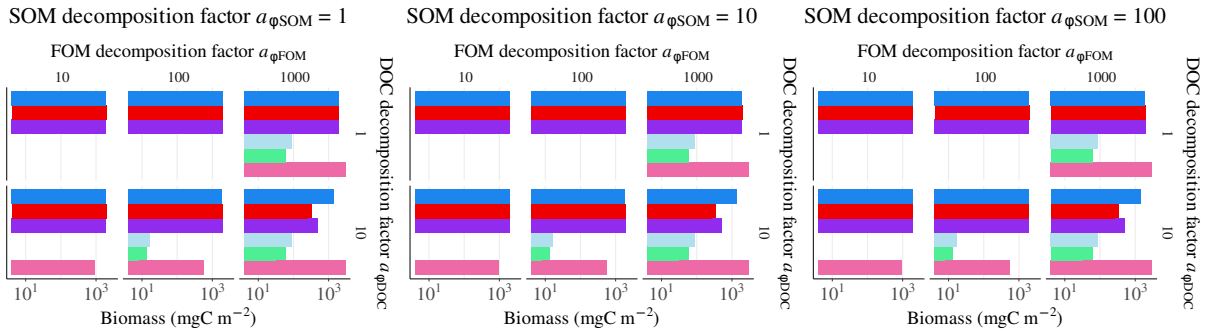

Figure S1-15: Biomass distribution among trophic groups depending on the decomposition factors of FOM ($a_{\varphi FOM}$), SOM ($a_{\varphi SOM}$) and DOC ($a_{\varphi DOC}$).

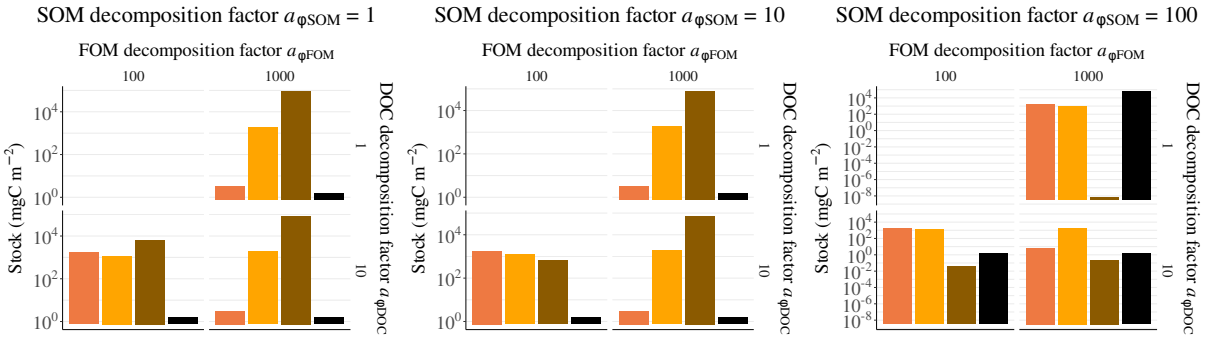

Figure S1-16: Detritus stocks depending on the decomposition factors of FOM ($a_{\varphi FOM}$), SOM ($a_{\varphi SOM}$) and DOC ($a_{\varphi DOC}$).

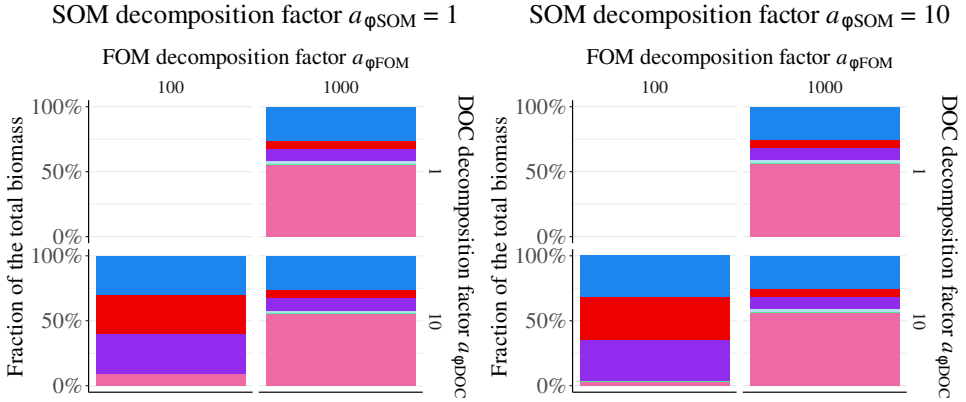

Figure S1-17: Relative biomass distribution depending on the decomposition factors of FOM ($a_{\varphi FOM}$), SOM ($a_{\varphi SOM}$) and DOC ($a_{\varphi DOC}$).

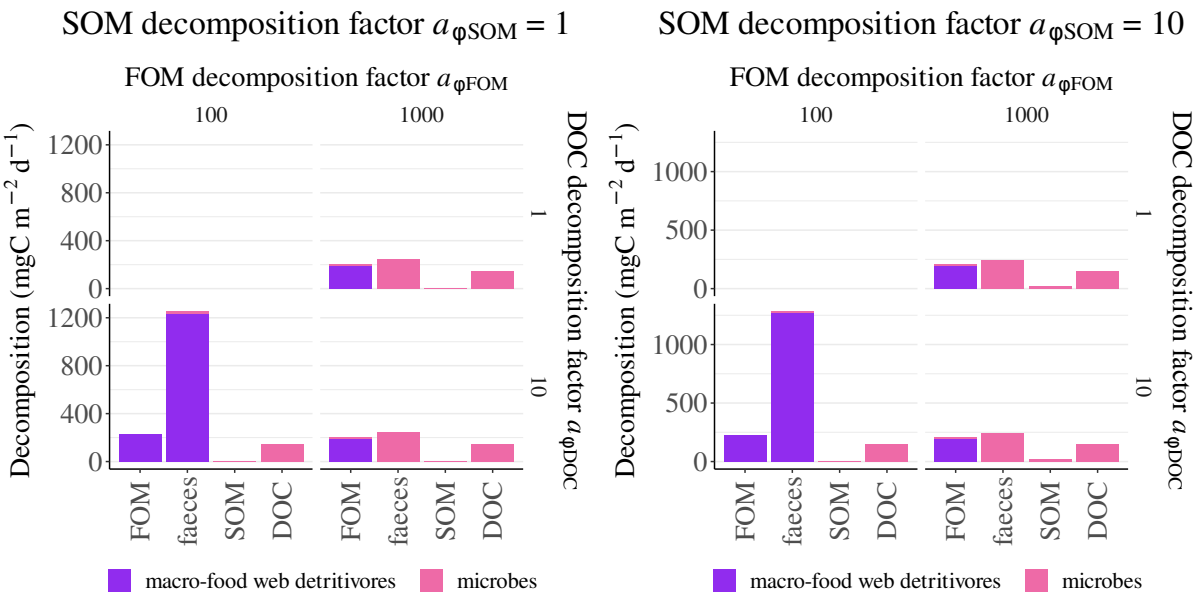

Figure S1-18: Decomposition of the different detritus classes depending on the decomposition factors of FOM ($a_{\varphi FOM}$), SOM ($a_{\varphi SOM}$) and DOC ($a_{\varphi DOC}$).

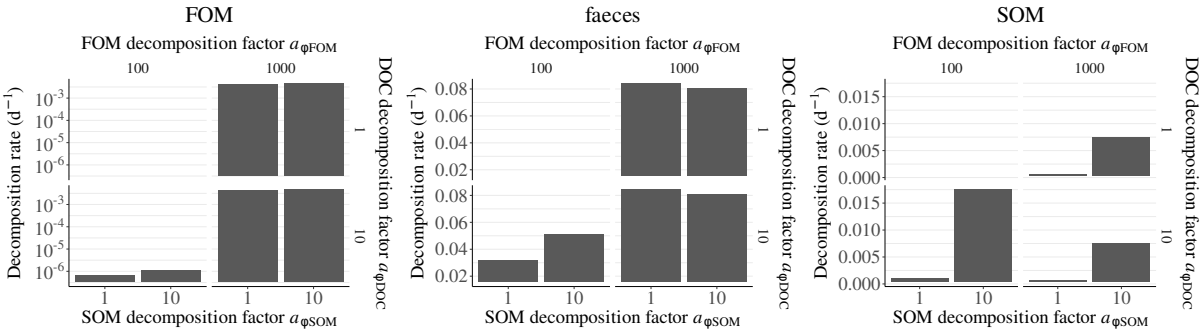

Figure S1-19: Decomposition rate by microbes of the different detritus classes depending on the decomposition factors of FOM ($a_{\varphi FOM}$), SOM ($a_{\varphi SOM}$) and DOC ($a_{\varphi DOC}$). As a reminder, the overall decomposition rates measured in Perveen et al. (2014) are equal to 0.032 d^{-1} for the SOM and 0.009 d^{-1} for the FOM.

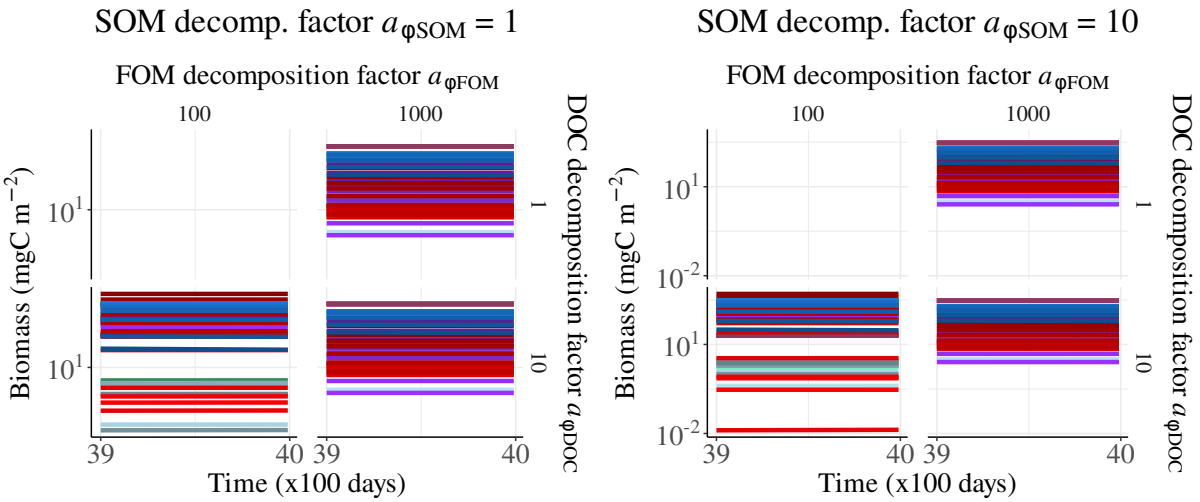

Figure S1-20: Time series over the 100 last days of the simulations depending on the decomposition factors of FOM ($a_{\varphi FOM}$), SOM ($a_{\varphi SOM}$) and DOC ($a_{\varphi DOC}$).

S1-2-3 Organic matter decomposition rate and radius of FOM

The efficient consumption of FOM by detritivores and faeces by microbes is an important feature of the model, which depends on the decomposition rate tuned by the factor $a_{\varphi FOM}$ and the radius of FOM pellets determining the available fraction of FOM for microbes (see Fig. S2-4). Therefore, we selected the values of these parameters to get a low decomposition of FOM and a high decomposition of faeces by microbes (Fig. S1-21B), and kept $a_{\varphi FOM} = 1000$ and $r_{FOM} = 10^6$ but the values corresponding the top right quarter of the graphs Fig. S1-21 would also match these requirements.

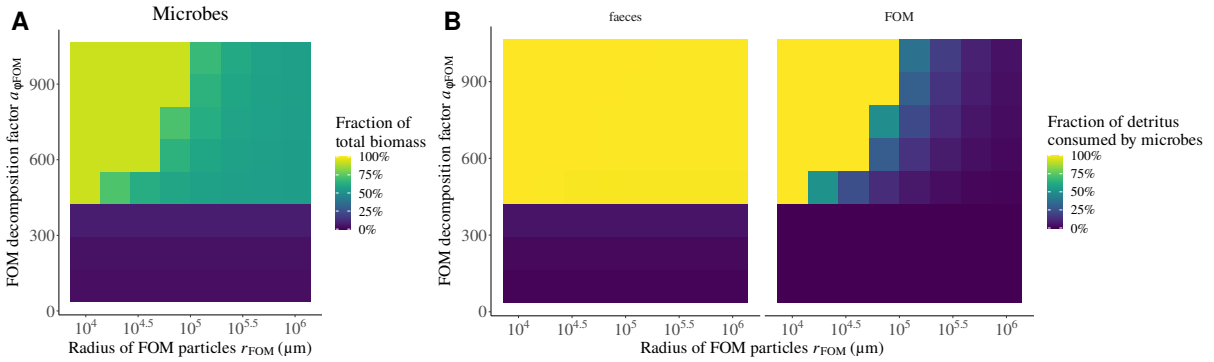

Figure S1-21: Crossed effects between the decomposition factors of FOM ($a_{\varphi FOM}$) and the radius of FOM particles r_{FOM}. **A)** Fraction of microbial biomass (ratio of the total microbial biomass to the total biomass). **B)** Fraction of decomposed FOM and faeces consumed by microbes.

S1-2-4 Self-regulation

The self-regulation of species represented by the consumer interference in the Beddington-DeAngelis functional response does not benefits from empirical measurements and it must be arbitrary stated. We decided to explore the values of its constants from the values of the attack rate. We keep $c_{0,prey} = 10^{5.5}$, $c_{0,pred} = 10^{6.25}$ and $s_c = -0.3$ according to the criteria summarised in Table S1-4.

Table S1-4: Distribution of the biomass for the two food web structures.

Criterion	$c_{0,prey}$	$c_{0,pred}$	s_c	Figure
Species persistence	-	-	> -0.4	S1-22
Large fraction of microbes	-	$\geqslant 10^{6.25}$	-0.3	S1-23
Abundance of macro-detritivores	-	$10^{6.25}$	-0.3	S1-23
Equilibrium	$\geqslant 10^{5.5}$	$\geqslant 10^{6.25}$	-0.3	S1-24
Final value	$\mathbf{10^{5.5}}$	$\mathbf{10^{6.25}}$	**-0.3**	

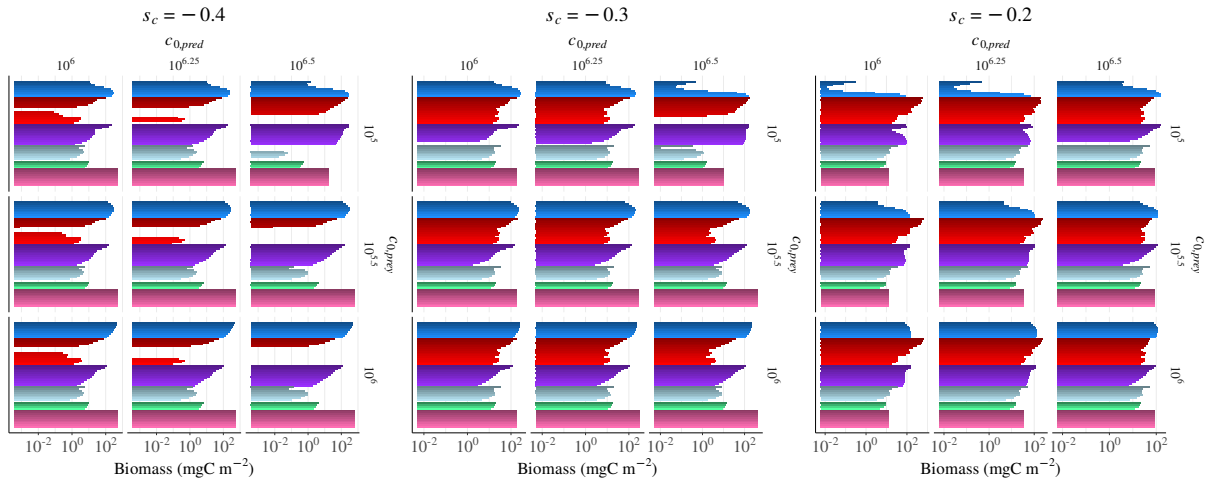

Figure S1-22: Biomass distribution among species depending on the normalisation constants $c_{0,prey}$ and $c_{0,pred}$ allometric scaling exponent s_c of the self-regulation.

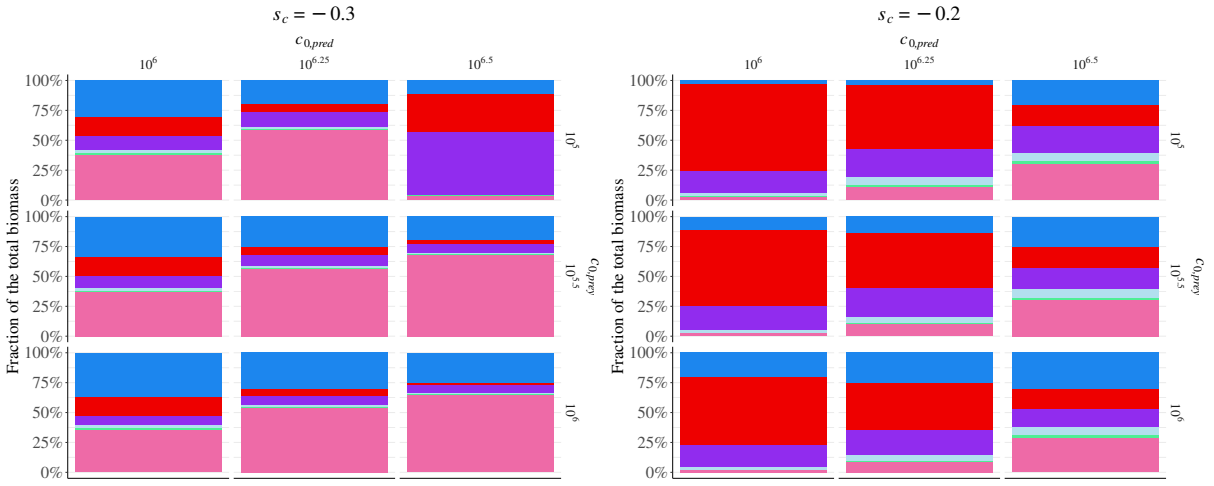

Figure S1-23: Relative biomass distribution among species depending on the normalisation constants $c_{0,prey}$ and $c_{0,pred}$ allometric scaling exponent s_c of the self-regulation.

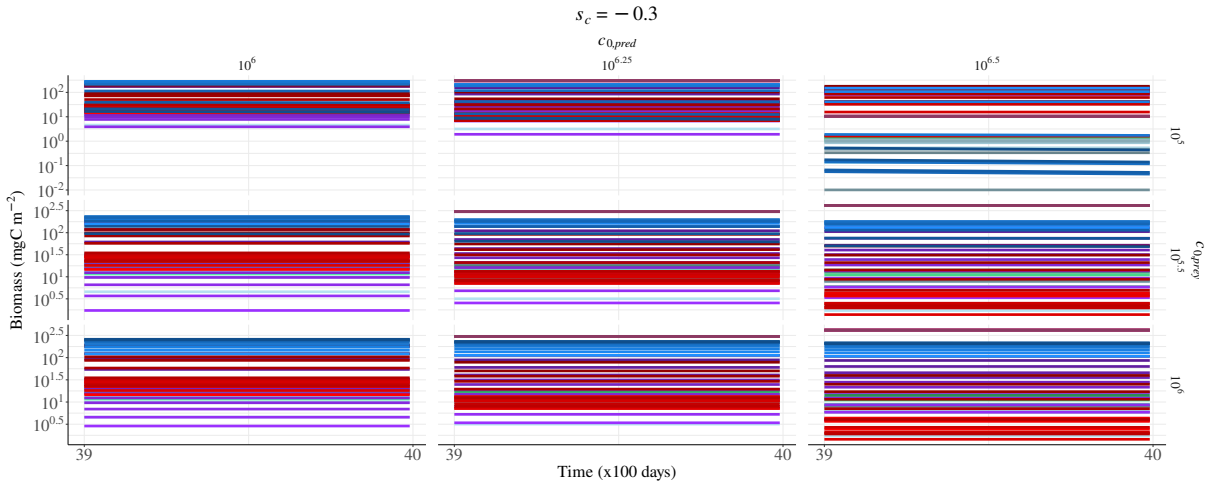

Figure S1-24: Time series over the 100 last days of the simulations depending on the normalisation constants $c_{0,prey}$ and $c_{0,pred}$ allometric scaling exponent s_c of the self-regulation.

S1-2-5 Microbe dormancy

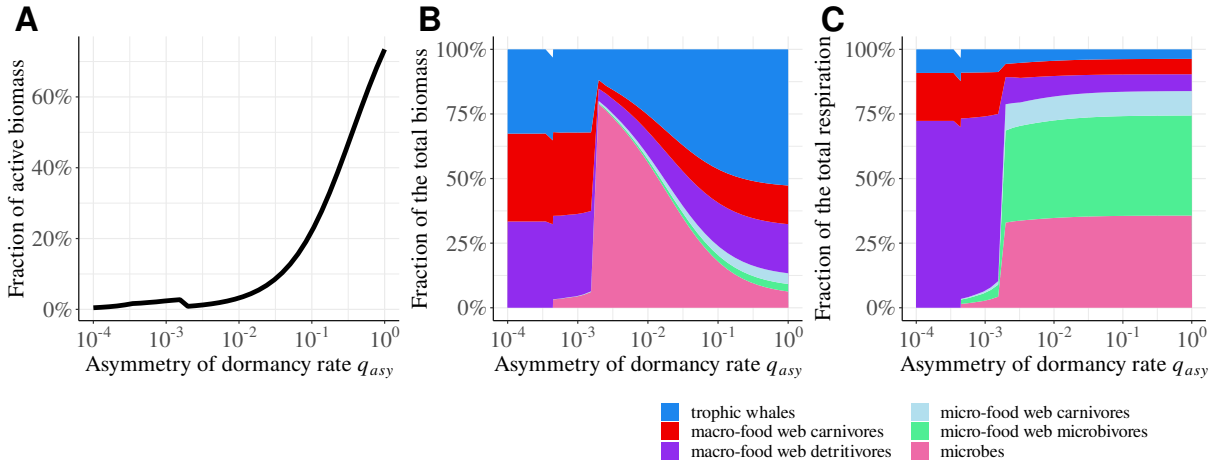

Figure S1-25: Effect of the dormancy asymmetry q_{asy}. **A)** Fraction of active microbes. **B)** Distribution of the biomass among the different trophic groups.

Microbial dormancy is needed for the ecosystem to accumulate an important microbial biomass according to empirical results (see Fig. 3D in the main text). Microbes become dormant or get activated depending on resource availability (see Appendix S2-5) but a baseline asymmetry between the rates is required for microbial biomass to strongly accumulate (Fig. S1-26B). We selected $q_{asy} = 10^{-2}$, which means that the activation rate is 100 times slower than the dormancy rate, which leads to 3.2% of microbes to be dormant (more than 70% without asymmetry with $q_{asy} = 1$, Fig. S1-26A). Note that the overall respiration is independent of q_{asy} that does not affect the active biomass of microbes, except for low values of q_{asy} that drive microbes to extinction. Therefore, the overall flows of C in the ecosystem are robust to q_{asy}.

S1-2-6 Feeding niche

The food web structure is determined by the feeding habits associated to each trophic group and the feeding niche of carnivores defined by the predator-prey body mass ratio in particular. The feeding niche is represented by a Gaussian distribution of mean 100 times smaller in average than predator i body mass (Brose et al., 2006) and an variance σ_i^M (see equation (S2-8) and Fig. S2-5). We kept $\sigma_i^M = 1$ for carnivores but other values do not change significantly the distribution of biomass among trophic groups (Fig. S1-26A) and the overall relationship between trophic levels and body mass (Fig. S1-26B). Having a higher variance σ_i^M only smoothers the distribution of trophic levels according to body mass because of the increased omnivory (Fig. S1-26C).

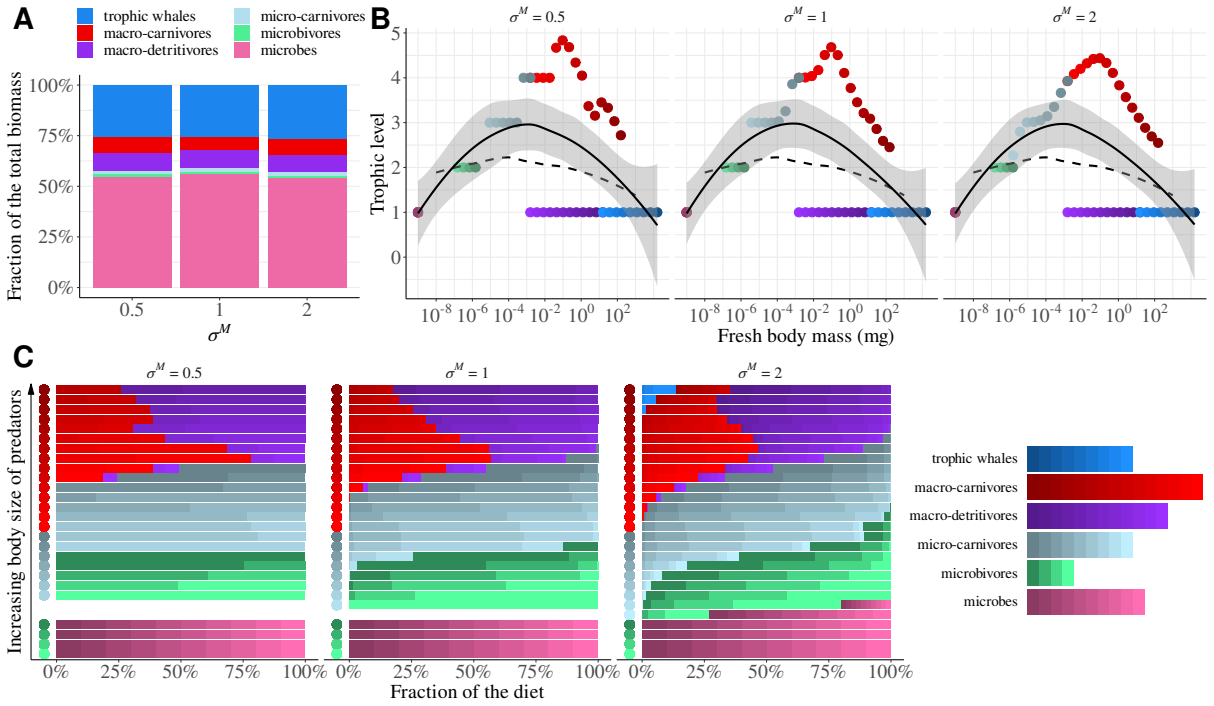

Figure S1-26: Effect of the width of the feeding niche σ^M of carnivores. **A)** Relative biomass distribution. **B)** Distribution of trophic levels depending on species fresh body mass for the two food web structures. Solid lines represent the average trophic level, the grey area the standard error and the dashed line the mean trophic level measured in boreal forests by Potapov et al. (2021). **D)** Proportion of each species in the diet of predators (represented by the dots).

S2 Complete model description

S2-1 Ecosystem description

We distinguish four detritus pools and six trophic groups forming two sub-food webs (Fig. 1A). The dissolved organic carbon (DOC) is the labile carbon pool such as root exudates that are absorbed by microbes. The soil organic matter (SOM) is the recalcitrant pool of soil carbon made of microbial dead materials that can be decomposed by microbes as well. The fresh organic matter (FOM) is made of the litter fall and the dead bodies of soil fauna. Finally, faeces are the nonassimilated fraction of the organic matter ingested by organisms. Following Potapov et al. (2021), we identify two sub-food webs: the micro- and the macro-food webs. The micro-food web contains microbes (bacteria and fungi) feeding on detritus, microbivores (*e.g.* protists and nematodes), their predators and micro-carnivores (*e.g.* nematodes and mites). The macro-food web contains macro-detritivores consuming FOM and faeces (*e.g.* springtails) and macro-carnivores (*e.g.* spiders). Trophic whales are large macro-detritivores (*e.g.* earthworms, woodlouse and millipedes) without predators from the macro-food web (Schwarzmüller et al., 2015). Potapov et al. (2021) actually consider trophic whales distinct from the macro-food web but because trophic whales are modelled with the same parameters as macro-detritivores (except their body size and the absence of predators), we include them in the macro-food web for the sake of simplicity.

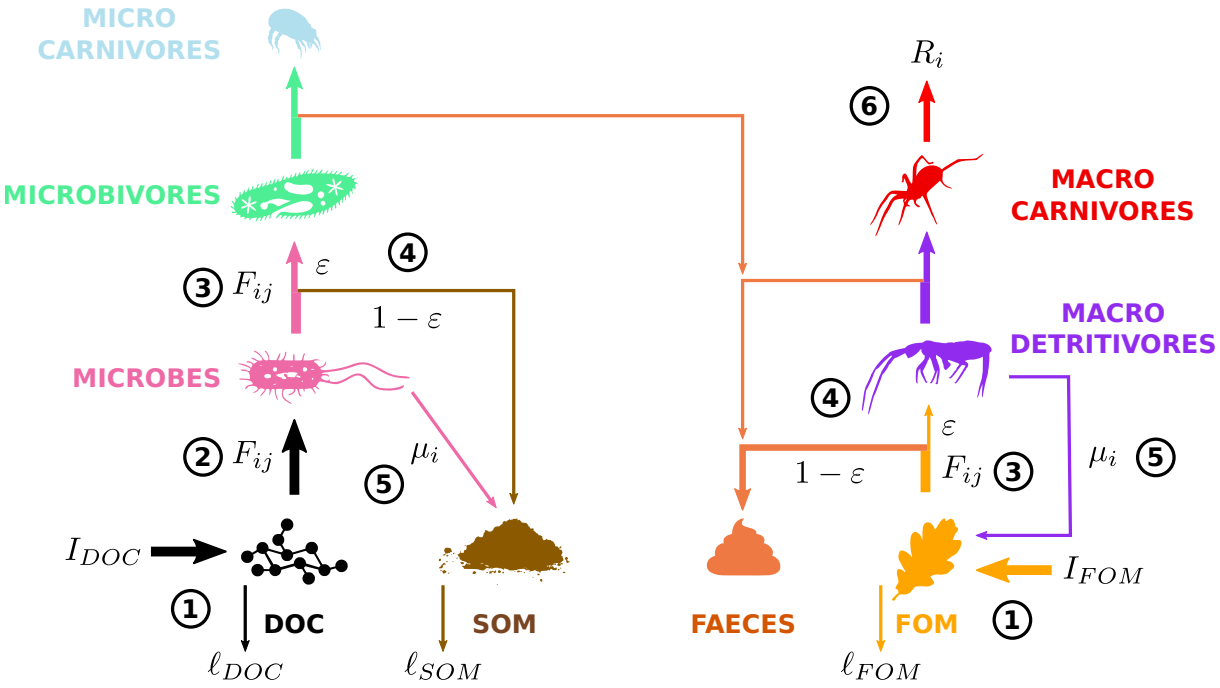

Figure S2-1: General representation of the flows in the ecosystem represented by arrows. All flows are not present but examples representative of each type of flow between the main compartments are represented.

All the flows in the ecosystem are carbon flows. The ecosystem is sustained by external inputs of DOC (I_{DOC}) and FOM (I_{FOM}), while DOC, SOM and FOM experience a leaching proportional to their stock (rates ℓ_{DOC}, ℓ_{SOM} and ℓ_{FOM}) but not faeces (Fig. S2-1 ①). SOM leaching is associated to burial and permanent storage of C in deep soil. Microbes consume the different detritus pools at a rate F_{ij} (Fig. S2-1 ② and equation (S2-11)). Animals (*i.e.* all nonmicrobe trophic groups) consume resources (detritus or organisms) at a rate F_{ij} (Fig. S2-1 ③ and equation (S2-14)) but they only assimilate a fraction ε of the ingested food (Table S2-1). The nonassimilated fraction $(1-\varepsilon)$ of ingested microbes is released as SOM while the it is released as faeces for all the other resources (Fig. S2-1 ④). All organisms die at an intrinsic rate μ_i (equation (S2-19)), microbes' corpses are converted into SOM and animals's corpses are converted into FOM (Fig. S2-1 ⑤). Organisms also lose biomass through metabolisms (equation (S2-9)), which lost as carbon dioxide by the system (Fig. S2-1 ⑥).

Table S2-1: Assimilation efficiency ε_{ij} of resource j by consumer i according to (Lang et al., 2017). The consumption of microbes is assumed to have the same efficiency as other organisms. Columns correspond to consumers and rows to resources. Note that trophic whales are not consumed by any carnivore because of their size.

Trophic group	Microbes	Microbivores	Micro carnivores	Macro detritivores	Macro carnivores	Trophic whales
DOC	1					
SOM	1					
faeces	1			0.18		0.18
FOM	1			0.18		0.18
Microbes		0.9		0.9		0.9
Microbivores			0.9			
Micro-carnivores			0.9		0.9	
Macro-detritivores					0.9	
Macro-carnivores					0.9	
Trophic whales						

The general equations of organism and detritus dynamics are expresses by equations (S2-1a) and (S2-1b) respectively.

$$\Delta B_i(t) = \underbrace{\sum_{j}^{\text{prey}} \varepsilon_{ij} \Delta B_{ij}(t)}_{\text{resource consumption}} - \underbrace{\sum_{j}^{\text{pred}} \Delta B_{ji}(t)}_{\text{predation}} - \underbrace{\Delta R_i(t)}_{\text{metabolism}} - \underbrace{\Delta \mu_i(t)}_{\text{mortality}} \tag{S2-1a}$$

$$\Delta B_i(t) = \underbrace{\Delta I}_{\text{input}} - \underbrace{\Delta \ell}_{\text{leaching}} + \underbrace{\sum_{k}^{\text{species}} \sum_{j}^{\text{prey}} (1 - \varepsilon_{kj}) \Delta B_{kj}(t)}_{\text{nonassimilated biomass}} - \underbrace{\sum_{k}^{\text{decomposers}} \Delta B_{ki}(t)}_{\text{decomposition}} + \underbrace{\sum_{j}^{\text{species}} \Delta \mu_j(t)}_{\text{mortality}} \tag{S2-1b}$$

According to (Harfoot et al., 2014), we model the variations of biomass $\Delta B_i(t)$ due to the demographic process X_i by an exponential function over a time step Δt.

$$\Delta X(t) = B_i(t)\Big[1 - \exp\Big(-\Delta t X_i(t)\Big)\Big] \tag{S2-2}$$

This ensures that the biomass lost by species i cannot exceed its biomass if the considered time step Δt is large (Fig. S2-2). Leaching $\Delta \ell$ follows equation (S2-2), while external inputs $\Delta I = I \Delta t$ because they are constant over time and do not depend on state variables.

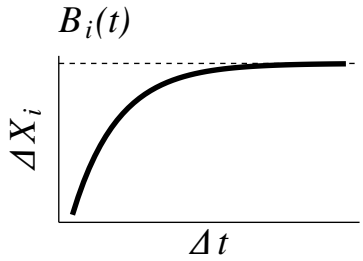

Figure S2-2: Biomass ΔB_j of resource j lost during a time step Δt. ΔB_j cannot exceed $B_j(t)$.

S2-2 Food web structure

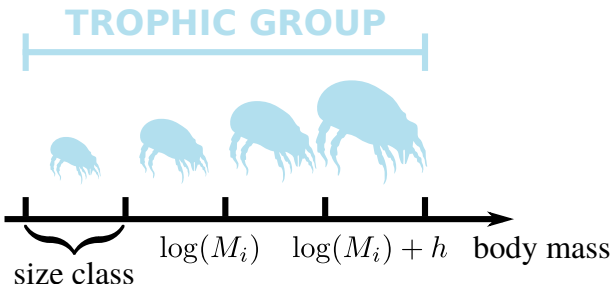

Figure S2-3: Trophic group divided into size classes along a log axis defined by the smallest size in class i M_i (mg fresh weight) and its width h on the log axis. Body masses are assumed to be log uniformly distributed in each size class.

Box S2-1: Body mass: from natural logarithm to logarithm with base 10

The body masses of soil organisms span over several orders of magnitude and we usually represent them on a logarithm with base 10 scale. However, equation (S2-3) uses natural logarithm transformations of body masses, thus, we get $\ln(M_{k+1}) = \ln(M_k) + \ln(10^h) = \ln(M_k) + h\ln(10)$.

Each trophic group is divided into size classes i in which we assume that body masses are log uniformly distributed between the boundaries $\log_{10}(M_i)$ and $\log_{10}(M_i) + h$, with h the width of the size class on a log scale (Fig. S2-3). Thus, there is a constant distribution density $1/h$ of body masses and the average individual body mass of size class i is equal to:

$$\overline{M_i} = \int_{\ln(M_i)}^{\ln(M_i)+h\ln(10)} \frac{e^x}{h\ln(10)} dx = \frac{M_i(10^h - 1)}{h\ln(10)} \tag{S2-3}$$

These average body masses $\overline{M_i}$ are used to calculate the demographic parameters according to allometric laws, trophic interactions and the size of faeces.

Indeed, animals, and detritivores in particular, fragment detritus by producing faeces whose size is proportional to their body mass. Here, faeces are modelled by spherical pellets of radius r_i (as other detritus, see), which is calculated according to the body mass of organisms (see Appendix S3-8 for the parameter calculation).

$$r_i = r_{int} + r_{slope}\overline{M_i} \tag{S2-4}$$

Microbes have access to the external layer r_a of the faecal pellets (Fig. S2-4A), which represents a fraction ϕ_i of detritus pool i.

$$\phi_i = 1 - \left(\frac{r_i - r_a}{r_i}\right)^3 \tag{S2-5}$$

The surface of detritus represents a microhabitat for microbes and each pool of detritus with a stock B_i hosts a fraction ϕ_i^{tot} of the total population of microbes.

$$\phi_i^{tot} = \frac{\phi_i B_i}{\sum_j \phi_j B_j} \tag{S2-6}$$

Therefore, when detritivores consume a quantity $B_{i,eaten}$ of detritus i, they also consume a biomass $B_{mic,eaten}$ of microbes whose total biomass is B_{mic} (Fig. S2-4B):

$$B_{mic,eaten} = \phi_i^{tot} \frac{B_{i,eaten}}{B_i} B_{mic} \tag{S2-7}$$

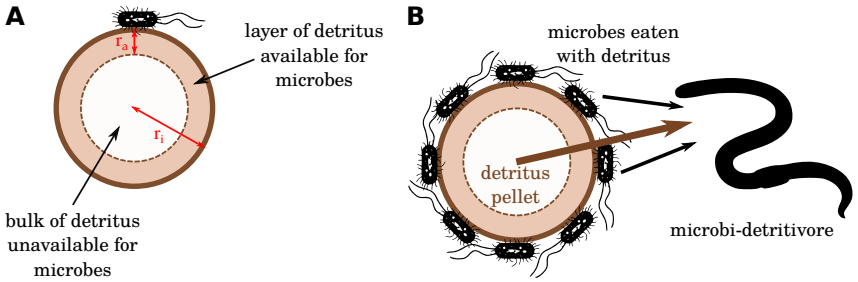

Figure S2-4: Representation of detritus pools by a collection of spherical pellets with a radius r_p. **A)** Only the external layer of pellets (r_a) is available for microbes while the bulk of detritus ($r_p - r_a$) remains protected. **B)** Microbi-detritivores eat the microbes living on the surface of detritus pellets while they consume detritus. The biomass of eaten microbes is proportional to the surface of consumed detritus.

The food web is structured according to the diet of each trophic group. The trophic interactions between predators and their prey are size-structured and follow the classic food web theory since micro- and macro-carnivores consume prey in average 100 times smaller (Brose et al., 2006). The interaction strength of each possible trophic link is modulated by the preference p_{ij} of consumers i for prey j depending on prey to predator body mass ratio.

$$p_{ij} = \exp\left(-\left(\frac{\ln\left(\overline{M_j}/\overline{M_i}\right) - \ln\left(\theta_i^M\right)}{\sigma_i^M}\right)^2\right) \tag{S2-8}$$

With θ_i^M the optimal prey to predator body mass ratio and σ_i^M the standard deviation, whose values for each trophic group are reported in Table S2-4.

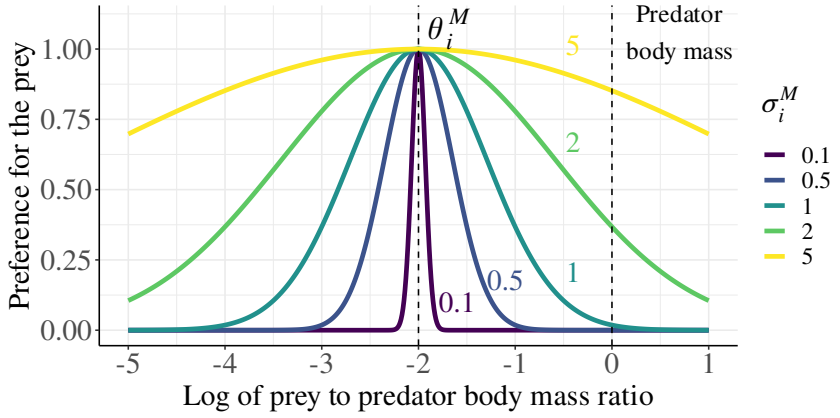

Figure S2-5: Preference of predator i for prey j depending on the log of prey to predator body mass ratio (M_j/M_i) for different mismatch tolerances σ_i^M with the optimal ratio θ_i^M (whose log is equal to -2, which means that prey are 100 times smaller than their predator according to Brose et al., 2006).

S2-3 Metabolism

The basal metabolic rate (or resting metabolic rate) corresponds to the metabolic rate measured in laboratory of resting organisms or nondividing microbes (Makarieva et al., 2005). According the metabolic theory of ecology (Brown et al., 2004), the mass-specific metabolic rate $R_i(t)$ follows a power-law relationship with body mass $\overline{M_i}$ and an exponential relationship with temperature T (Ehnes et al., 2011).

$$R_i(t) = R_0 \overline{M_i}^{s_R} \exp\left(\frac{-E_R}{k_B T}\right) \tag{S2-9}$$

R_0 is the mass- and temperature-independent constants, s_R is an allometric exponent, E_R is the aggregated activation energy of metabolic reactions and k_B is the Boltzmann constant. The values of these parameters have been calculated for the main classes of soil organisms (microbes, mesofauna and

macrofauna) according to Johnston and Sibly (2018). The detail of the statistical analysis and unit conversion are in Appendix S3-4 and the values of the parameters for each trophic group are reported in Table S2-4.

According to equation (S2-2), the biomass loss $\Delta R_i(t)$ through respiration of the active fraction of the population $\zeta_i(t)$ over a time step Δt is defined by:

$$\Delta R_i(t) = \zeta_i(t) B_i(t) \Big[1 - \exp\Big(- \Delta t R_i(t) \Big) \Big] \tag{S2-10}$$

S2-4 Consumption by microbes

Microbe species i take up carbon from the detritus pools j according to a Michaelis-Menten functional responses and depending on the available fraction of the pool ϕ_j (equation (S2-5) and Fig. S2-4A):

$$F_{ij}(t) = \frac{\phi_j \varphi_{Cj}^{max} \zeta_i(t) B_i(t)}{K_{Cj} + \phi_j B_j} \tag{S2-11}$$

Since we consider that degrading the FOM and the faeces requires the same enzymatic activity (they both represent labile carbon), we assume they share the same instantaneous uptake function:

$$F_{ij}(t) = \frac{\phi_j \varphi_{Cj}^{max} \zeta_i(t) B_i(t)}{K_{Cj} + \underset{\text{FOM+faeces}}{\sum_k \phi_k B_k}} \tag{S2-12}$$

The half-saturation constant K_C and maximal absorption rate φ_C^{max} are temperature (T) dependent according to German et al. (2012) and Wieder et al. (2014):

$$K_C = a_{K_C} K_{C0} \exp(s_{K_C} T) \qquad \varphi_C^{max} = a_{\varphi_C} \varphi_{C0} \exp(s_{\varphi_C} T) \tag{S2-13}$$

K_{C0} and φ_{C0} are scaling coefficients, s_{K_C} and s_{φ_C} are temperature scaling coefficients and a_{K_C} and a_{φ_C} are tuning coefficients necessary to approach realistic stocks of dead organic matter (Appendices S1-2-1 and S1-2-2). The detail of the unit conversion are in Appendix S3-7 and the values of the parameters are reported in Table S2-4.

The quantity of detritus consumed by each microbe species is calculated according to equations (S2-16) and (S2-17).

S2-5 Consumption by animals

The instantaneous loss of biomass $F_{ij}(t)$ of resource j consumed by consumer i is calculated according to the Beddington-DeAngelis functional response (Beddington, 1975; DeAngelis et al., 1975).

$$F_{ij}(t) = \frac{\zeta_i(t) p_{ij} a_{ij} B_i(t)}{1 + \underset{k}{\overset{\text{prey}}{\sum}} \zeta_k(t) p_{ik} a_{ik} h_{ik} B_k(t) + c_i B_i(t)} \tag{S2-14}$$

p_{ij} is the preference of consumer i for resource j (equation (S2-8)). Only the fraction $\zeta_i(t)$ of active consumers effcetively consume the fraction $\zeta_k(t)$ of active prey because we assume dormant organisms to be protected against predation. The attack rate a_{ij} and the handling time h_{ij} are both mass- and temperature-dependent according to Li et al. (2018). The interference c_i is defined based on the parameters of the attack rate and some are also hand tuned (Appendix S1-2-4) because of the lack of data.

$$a_{ij} = a_0 \overline{M_i}^{s_a} \exp\left(\frac{-E_a}{k_B T}\right) \qquad h_{ij} = h_0 \overline{M_i}^{s_h} \exp\left(\frac{-E_h}{k_B T}\right) \qquad c_i = c_0 \overline{M_i}^{s_c} \exp\left(\frac{-E_c}{k_B T}\right) \tag{S2-15}$$

a_0, h_0 and c_0 are the normalisation constants, s_a, s_h and s_c are the allometric scaling exponents, E_a, E_h and E_c are the activation energies, k_B is Boltzmann's constant and T is the temperature. The detail

of the statistical analysis and unit conversion are in Appendix S3-6 and the values of the parameters for each trophic group are reported in Table S2-4.

Following Harfoot et al. (2014), the total of biomass lost $\Delta B_{\cdot j}(t)$ by resources j through consumption over a time step Δt is defined by:

$$\Delta B_{\cdot j}(t) = \zeta_j(t) B_j(t) \left[1 - \exp\left(-\Delta t \sum_i^{\text{pred}} F_{ij}(t)\right)\right] \tag{S2-16}$$

Then, the biomass of resource j eaten by each consumer i is defined by:

$$\Delta B_{ij}(t) = \Delta B_{\cdot j}(t) \times \frac{F_{ij}(t)}{\sum_k^{\text{pred}} F_{kj}(t)} \tag{S2-17}$$

Microbivory

Macro-detritivores and trophic whales i consume the microbe species j (both active and dormant) growing on the eaten detritus k (Fig. S2-4B). The biomass of consumed microbes $\Delta B_{ij}(t)$ is proportional to total surface of each detritus pool ϕ_k^{tot} according to equation (S2-6) and to the consumed fraction of each detritus pool $\Delta B_{ik}(t)/B_k(t)$.

$$\Delta B_{ij}(t) = B_j(t) \sum_k^{\text{detritus}} \phi_k^{tot} \frac{\Delta B_{ik}(t)}{B_k(t)} \tag{S2-18}$$

Intrinsic mortality and self-regulation

Organisms have an intrinsic mortality rate due to senescence $\mu_i(t)$ following a power-law relationship with body mass and an exponential relationship with temperature T as reported by McCoy and Gillooly (2008):

$$\mu_i(t) = \mu_0 \overline{M_i}^{s_\mu} \exp\left(\frac{-E_\mu}{k_B T}\right) \tag{S2-19}$$

μ_0 is the mass- and temperature-independent constants, E_μ is the activation energy, s_μ the allometric exponent and k_B the Boltzmann constant. The detail of the statistical analysis and unit conversion are in Appendix S3-5 and the values of the parameters are reported in Table S2-4.

In addition, microbes experience self-regulation, which is a density-dependent mortality rate (*e.g.* allelopathy or bacterophages) and whose allometric parameters are chosen equal to those of the attack rate because of the lack of data in the literature. D_0 is assumed to be equal to 1 to keep self-regulation low.

$$D_i(t) = D_0 \overline{M_i}^{s_D} \exp\left(\frac{-E_D}{k_B T}\right) \tag{S2-20}$$

The overall mortality $\Delta\mu_i$ over a time step Δt is defined as follow:

$$\Delta\mu_i(t) = B_i(t) \left(1 - e^{-(\mu_i(t) + D_i(t))\Delta t}\right) \tag{S2-21}$$

Dormancy of microbes

Microbes switch from dormant to active states (and vice versa) at a transition rate $q_i^{act} Q$ ($q_i^{dorm} Q$) with Q the maximum transition rate and q_i^{act} and q_i^{dorm} the sensitivity functions of carbon balance controlling activation and dormancy respectively (Panikov and Sizova, 1996; Stolpovsky et al., 2011; Manzoni et al., 2014; Wang et al., 2014).

$$q_i^{act} = \frac{\sum_{j}^{\text{prey}} \varepsilon_{ij} \Delta B_{ij}(t)}{\underbrace{\sum_{j}^{\text{prey}} \varepsilon_{ij} \Delta B_{ij}(t)}_{(1)} + \underbrace{\Delta R_i(t)}_{(2)}} \qquad q_i^{dorm} = 1 - q_i^{act} = \frac{\Delta R_i(t)}{\sum_{j}^{\text{prey}} \varepsilon_{ij} \Delta B_{ij}(t) + \Delta R_i(t)} \tag{S2-22}$$

These functions depend on the biomass gained through the consumption of resources (1) and the loss through respiration (2) (equation (S2-1a)).

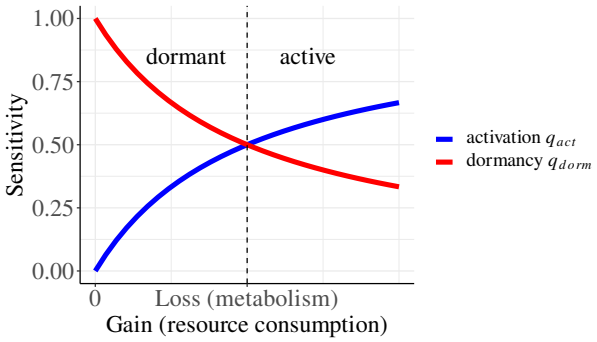

Figure S2-6: Functions modulating the transition rate between active and dormant states. q_i^{act} and q_i^{dorm} are symmetric and equal when losses by respirations are compensated by gains from resource consumption ($G_i = R_i$), which means that more microbes become dormant if $G_i < R_i$ or active if $H_i > R_i$.

Let us note B_i^{act} and B_i^{dorm} the biomasses of microbe species i, which are active and dormant respectively, and $B_i = B_i^{act} + B_i^{dorm}$ the total biomass of microbe species i. Dormant microbes do not consume resources and their metabolism is shut down (no carbon loss due to respiration), they suffer basal mortality and are protected from predation. In addition, we consider that the activation rate is asymmetric to the dormancy rate by a factor q_{asy}, which enables a large fraction of microbes to stay dormant (Fig. S1-25). To assess the fraction of microbes that is active, we only consider dormancy and activation as demographic processes.

$$\frac{dB_i^{act}}{dt} = -B_i^{act} q_i^{dorm} Q + B_i^{dorm} q_{asy} q_i^{act} Q \tag{S2-23a}$$

$$\frac{dB_i^{dorm}}{dt} = B_i^{act} q_i^{dorm} Q - B_i^{dorm} q_{asy} q_i^{act} Q \tag{S2-23b}$$

Then, we define $\zeta_i = B_i^{act}/B_i$ the fraction of microbe species i that is active. At equilibrium, we have $B_i^{act}/B_i^{dorm} = q_{asy} q_i^{act}/q_i^{dorm}$ and $\zeta_i = q_{asy} q_i^{act}/(q_{asy} q_i^{act} + q_i^{dorm})$. Since we can consider B_i constant, we can easily calculate the dynamics of ζ_i.

$$\frac{d\zeta_i}{dt} = \frac{1}{B_i}\frac{dB_i^{act}}{dt} = \frac{Q}{B_i}(B_i^{dorm} q_{asy} q_i^{act} - B_i^{act} q_i^{dorm}) \tag{S2-24a}$$

$$= Q\Big((1-\zeta_i) q_{asy} q_i^{act} - \zeta_i q_i^{dorm}\Big) \tag{S2-24b}$$

$$= \underbrace{Q\Big(q_{asy} q_i^{act} + (1 - q_i^{act})\Big)}_{\text{overall rate of change}} \underbrace{\Big(\frac{q_{asy} q_i^{act}}{q_{asy} q_i^{act} + 1 - q_i^{act}} - \zeta_i\Big)}_{\text{expected equilibrium}} \tag{S2-24c}$$

Therefore, the variation of the fraction of dormant microbes $\Delta\zeta_i$ can be computed as follows:

$$\Delta\zeta_i = \left(\frac{q_{asy} q_i^{act}}{q_{asy} q_i^{act} + 1 - q_i^{act}} - \zeta_i\right)\left(1 - \exp\Big(-\Delta t Q\Big(q_{asy} q_i^{act} + (1 - q_i^{act})\Big)\Big)\right) \tag{S2-25}$$

Parameters

Table S2-2: Characteristics of the main trophic groups.

Parameter	Microbes	Microbivores	Micro-carnivores	Macro-detritivores	Macro-carnivores	Trophic whales
Initial density	1×10^4	10	10	1×10^5	1×10^4	1×10^5
M_{min} (log10)	-9	-7	-6	-3	-3	1
M_{max} (log10)	-9	-6	-3	1	2	4
# size class	10	4	9	12	15	9
θ_i^M	-	0.01	0.01	0.1	0.01	0.1
σ_i^M	-	100	1	10	1	10
$\ln(R_0)$	25.25	20.27	20.27	2.2	2.2	2.2
s_R	-0.14	-0.35	-0.35	-0.3	-0.3	-0.3
E_R	0.75	0.63	0.63	0.64	0.64	0.64
c_0	-	$10^{6.25}$	$10^{6.25}$	$10^{5.5}$	$10^{6.25}$	$10^{5.5}$
a_h	-	1	1	0.1	1	0.1

Table S2-3: Value of the decomposition parameters of detritus by microbes. The details of unit conversion and references are given in Appendix S3-7.

Parameter	DOC	FOM	faeces	SOM
K_C0	1.1×10^{-5}	3.2×10^{-3}	3.2×10^{-3}	3.2×10^{-3}
φ_{C0}	7.09×10^{-8}	8.87×10^{-11}	8.87×10^{-11}	3.03×10^{-10}
s_K	0.034	0.034	0.034	0.034
s_φ	0.063	0.063	0.063	0.063
a_K	0.01	0.001	0.001	0.001
a_φ	10	1000	1000	10
r_i	-	1×10^6	equation (S2-5)	10
I	150	300	0	0
ℓ	0.0026	0.001	0	0.001

Table S2-4: Table of state variables and parameters.

Symbol	Description	Value	Units	Reference
B_i	biomass	-	$\mathrm{mgC\,m^{-2}}$	-
ϕ_i	fraction of accessible	equation (S2-5)	dimensionless	-
r_i	radius of detritus pellet i	equation (S2-4)	µm	-
q_{act}	activation of microbes	equation (S2-22)	dimensionless	-
q_{dorm}	dormancy of microbes	equation (S2-22)	dimensionless	-
ζ_i	fraction of active microbes	equation (S2-25)	dimensionless	-
T	temperature	288.15	K	-
k_B	Boltzmann constant	8.62×10^{-5}	$\mathrm{eV\,K^{-1}}$	-
θ^M	resource-consumer body mass ratio	Table S2-2	dimensionless	Brose et al., 2006
σ^M	resource pref. standard dev.	Table S2-2	dimensionless	assumed
ε_{ij}	assimilation efficiency	Table S2-1	dimensionless	Lang et al., 2017
R_0	metabolic scaling const.	Table S2-2	$\mathrm{J\,h^{-1}}$	Johnston and Sibly, 2018
s_R	metabolic allometric exp.	Table S2-2	dimensionless	Johnston and Sibly, 2018
E_r	activation energy	Table S2-2	eV	Johnston and Sibly, 2018
μ_0	normalisation const.	5.52×10^{-3}	$\mathrm{yr^{-1}\,mgC^{-}}^{s_\mu}$	McCoy and Gillooly, 2008
s_μ	allometric scaling exp.	-0.26	dimensionless	McCoy and Gillooly, 2008
E_μ	activation energy	0.83	eV	McCoy and Gillooly, 2008
D_0	self-regulation scaling const.	1	$\mathrm{m^2\,mgC^{-1-1-}}^{s_D}$	assumed
s_D	self-regulation allometric exp.	-0.49	dimensionless	assumed
E_D	activation energy	0.43	eV	assumed
c_0	attack rate scaling const.	Table S2-2	$\mathrm{m^2\,mgC^{-1-1-}}^{s_c}$	assumed
s_c	attack rate allometric exp.	-0.3	dimensionless	assumed
E_c	activation energy	0.43	eV	assumed
a_0	attack rate scaling const.	4.67×10^5	$\mathrm{m^2\,mgC^{-1-1-}}^{s_a}$	Li et al., 2018
s_a	attack rate allometric exp.	-0.49	dimensionless	Li et al., 2018
E_a	activation energy	0.43	eV	Li et al., 2018
a_a	tuning coefficient	1	dimensionless	assumed
h_0	handling time scaling const.	7.22×10^{-6}	$\mathrm{d\,mgC_{pred}\,mgC_{prey}^{-1}\,mgC^{-}}^{s_h}$	Li et al., 2018
s_h	handling time allometric exp.	0.24	dimensionless	Li et al., 2018
E_h	activation energy	-0.31	eV	Li et al., 2018
a_a	tuning coefficient	Table S2-2	dimensionless	assumed
K_{C0}	half-saturation const.	Table S2-3	$\mathrm{mgC\,m^{-2}}$	Appendix S3-7
s_K	half-saturation regression coef.	Table S2-3	$\mathrm{K^{-1}}$	Appendix S3-7
a_K	tuning coefficient	Table S2-3	dimensionless	assumed
φ_{C0}	max. decomposition const.	Table S2-3	$\mathrm{mgC\,mgC^{-1}\,d^{-1}}$	Appendix S3-7
s_φ	max. decomposition regression coef.	Table S2-3	$\mathrm{K^{-1}}$	Appendix S3-7
a_φ	tuning coefficient	Table S2-3	dimensionless	assumed
Q	switch rate of microbes	24	$\mathrm{d^{-1}}$	Stolpovsky et al., 2011
q_{asy}	asymmetry in switch rate	0.01	dimensionless	assumed
r_a	radius of available detritus	10	µm	assumed
r_{int}	faces size constant	9.81	µm	Appendix S3-8
r_{slope}	faeces size regression coef.	0.073	$\mathrm{\mu m\,mgC^{-1}}$	Appendix S3-8
I	external input	Table S2-3	$\mathrm{mgC\,d^{-1}}$	Appendix S3-9
ℓ	leaching rate	Table S2-3	$\mathrm{d^{-1}}$	Appendix S3-9

Simulations

Simulation are run over 4000 days with a time step $\Delta t = 0.01$, which enables the system to reach a stable equilibrium (Fig. S1-11). We average the outputs of the model over the last 100 days of the simulations and consider a species as extinct if its biomass falls bellow $1 \times 10^{-10}\,\mathrm{mgC\,m^{-2}}$.

S3 Complementary methods

S3-1 Food web structure

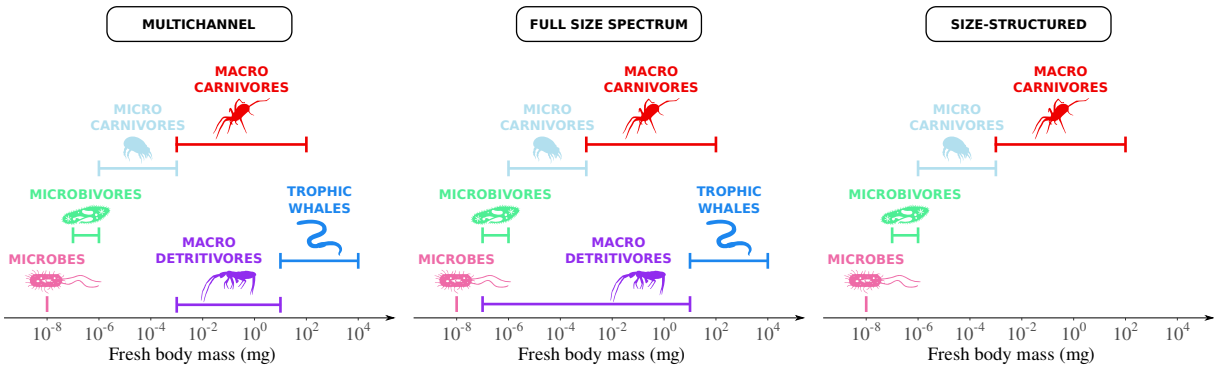

Figure S3-1: Trophic groups and their body size distribution in each food web structure. The **multichannel** model is representative of the structure described by Potapov et al. (2021). The **full size spectrum** model is a multichannel model in which the body mass interval of detritivorous invertebrates spans over both the micro- and the macro-food webs. The **size-structured** model is a classic Allometric Diet Breadth Model in which the body size is fully correlated to the trophic level.

S3-2 Statistical analysis

We have reused the same statistical analysis as the paper from which we picked up the datasets. The analysis we made by our own were performed with the *Anova* function of the *car* package on *R* 4.1.2.

S3-3 General unit conversion

First of all, the units of parameters in literature are usually wrong although we believe the numerical values are correct. We have had to correct the units from several papers and we beg ecologists in the future for being extremely careful when writing down the parameters they have fitted.

The allometric scaling of biological rates relies on relation between flows of matter and body mass. Flows must be in carbon for us to implement properly stoichiometric constrains but body mass are usually expressed as fresh weight. Thus, we convert all the biomasses and detritus stocks into carbon (Table S3-2) thanks to conversion factors (Table S3-1). In addition, biological rates are usually expressed as rates per individual and we must convert them into rates per unit of biomass (mass specific rates).

Table S3-1: Factors converting the units of the parameters collected from the literature.

Conversion	Value	Reference
organism dry:fresh weight ratio	0.2	Makarieva et al., 2005; Ehnes et al., 2011 Johnston and Sibly, 2018
organism C:dry weight ratio	0.42	Andrieux et al., 2021
J:mL O_2 ratio	20.1	Peters, 1983; Johnston and Sibly, 2018
mgC:mL O_2 ratio	0.5363	Lampert, 1984; Johnston and Sibly, 2018
volume of soil	$0.1\,m^3\,m^{-2}$	-
bacteria cell mass	1×10^{-9} mg	Makarieva et al., 2005
carbon molar mass	$12.011\,g\,mol^{-1}$	-
nitrogen molar mass	$14.0067\,g\,mol^{-1}$	-
water:soil volume ratio (moisture)	0.2	Heathman et al., 2003
soil bulk	$1.4\,g\,cm^{-3}$	Heathman et al., 2003

Table S3-2: Units used in the model.

Dimension	Desired units
Compartment mass	mgC
Body mass	mgC
Flows	mgC
Temperature	K
Time	day
Surface	m^2

S3-4 Metabolic rate unit conversion

We used the metabolic data set compiled by Johnston and Sibly (2018) (available at the following link: https://doi.org/10.5061/dryad.416kv03). It gathers the dataset of Ehnes et al. (2011), itself including the data from the meta-analyses of Meehan (2006) and Chown et al. (2007) together with measurements for acari, collembola, enchytraeidae, centipedes, millipedes, isopods, spiders, ants, beetles, termites and earthworms (n =3,399) performed by Ehnes et al. (2011) themselves. In addition, Johnston and Sibly (2018) compiled data for bacteria from Makarieva et al. (2005) (n =56), protozoa from Laybourn and Finlay (1976) and Fenchel and Finlay (1983) (n =143), nematodes from Klekowski et al. (1972) and Ferris et al. (1995) (n =105) and enchytraeidae from Nielsen (1961) (n =58).

Johnston and Sibly (2018) used fresh mass (mg) and standard individual metabolic rate per hour ($J\,h^{-1}$), using a dry to fresh mass ratio of 0.2 (Ehnes et al., 2011), 1 mL O_2 = 20.1 J (Peters, 1983) and 1 mL O_2 = 0.5363 mgC (Lampert, 1984). We redid the statistical analysis performed by Johnston and Sibly (2018) to convert the individual metabolic rates into mass-specific metabolic rates and the parameters into the appropriate units according to Table S3-3 to get the values used in our model summarised in Table S3-4.

$$R_i = R_0 M_i^{s_R} \exp\left(\frac{-E_R}{k_B T}\right) \tag{S3-1}$$

Table S3-3: Conversion of the units used in Johnston and Sibly (2018) to the units used in our model.

Parameter	Original units	Converted unites
R_i	$J\,h^{-1}\,Ind^{-1}$	$mgC\,mgC^{-1}\,d^{-1}$
R_0	$J\,h^{-1}\,Ind^{-1}\,mg^{-s_R}$	$d^{-1}\,mgC^{-s_R}$
M_i	mg (fresh)	mgC

Table S3-4: Original values of metabolic parameters calculated by Johnston and Sibly (2018) and their converted values.

	Original values			Converted values		
	Microbes	Mesofauna	Macrofauna	Microbes	Mesofauna	Macrofauna
$\ln(R_0)$	25.27	21.23	20.90	27.25	20.27	22.20
s_R	0.87	0.66	0.71	-0.14	-0.35	-0.30
E_R	0.74	0.68	0.64	0.75	0.63	0.64

Johnston and Sibly (2018) assessed soil respiration by calculating the mass-specific metabolic rate R_i with the allometric parameters reported in Table S3-4 and the average body mass of the main soil fauna groups (*e.g.* bacteria, nematodes and termites, Fig. S3-2B). Then, this mass-specific metabolic rate is simply multiplied by the average biomass of each group.

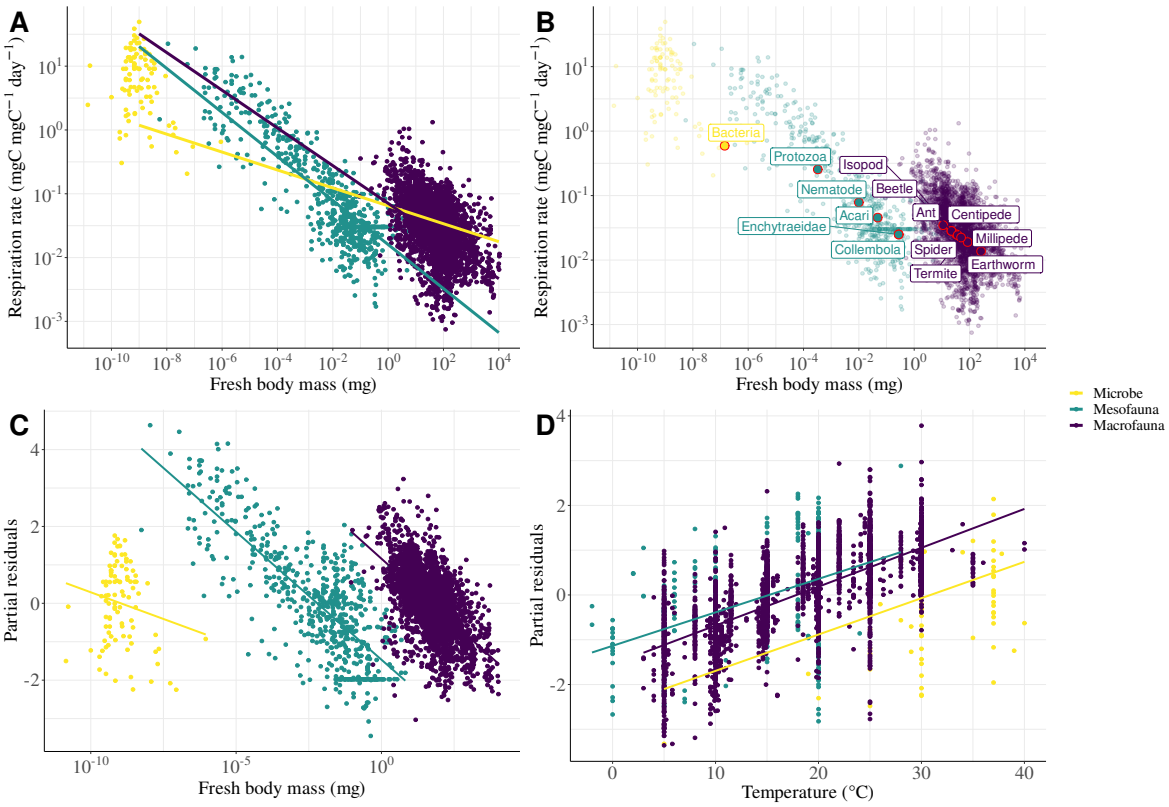

Figure S3-2: Calculation of the allometric parameters of the mass specific metabolic rate according to trophic groups from the data of Johnston and Sibly (2018). **A)** Distribution of the mass specific metabolic rate depending on body size. **B)** Mean body mass for each main taxa of the soil fauna (red circled points). **C)** Residuals of the mass specific metabolic rate depending on body mass after temperature correction. **D)** Residuals of the mass specific metabolic rate depending on temperature after body mass correction correction.

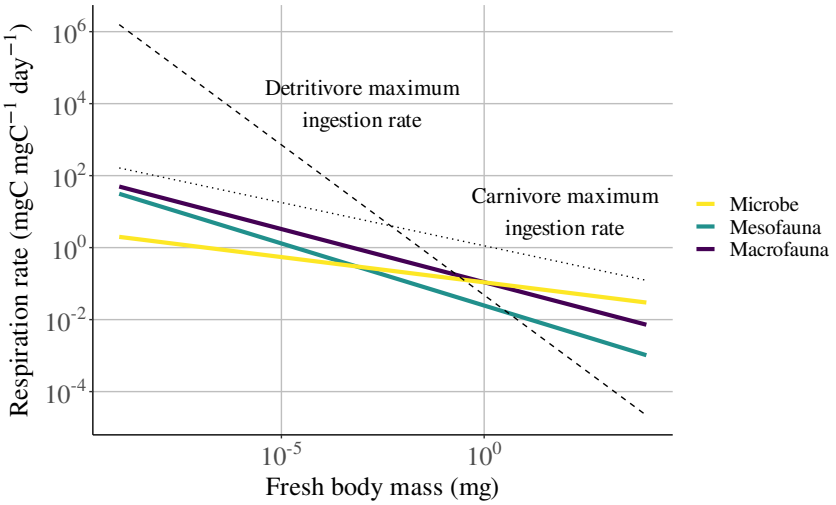

Figure S3-3: Mass specific metabolism and maximum ingestion rate depending on fresh body mass and trophic group (T =288.15 K).

S3-5 Intrinsic mortality rate unit conversion

We used the data set gathered by McCoy and Gillooly (2008) (available in their supporting information), which contains the natural mass-specific mortality rate of five taxonomic groups: invertebrates (128 species), fish (168 species), plants (278 species including phytoplankton), mammals (361 species), birds (600 species), which span a broad range of body temperatures (from 1 to 40 °C) and body masses (1.4×10^{-14} to 1.5×10^{8} g). We only kept the data relative to invertebrates and removed the observations

with a mortality rate equal to zero. The authors considered a dry to fresh weight ratio of 0.25 and we corrected their dry masses to get a ratio of 0.2 for the sake of consistency with the analysis of the other datasets.

$$\mu_i = \mu_0 M_i^{s_\mu} \exp\left(\frac{-E_\mu}{k_B T}\right) \tag{S3-2}$$

Table S3-5: Conversion of the units used in McCoy and Gillooly (2008) to the units used in our model.

Parameter	Original units	Converted value and unites
μ_i	yr^{-1}	d^{-1}
μ_0	$\mathrm{yr}^{-1}\,\mathrm{g}^{-s_\mu}$	$5.52 \times 10^{-3}\,\mathrm{d}^{-1}\,\mathrm{mgC}^{-s_\mu}$
s_μ	-	-0.26
E_μ	eV	0.83 eV

S3-6 Functional response unit conversion

Resource consumption by animals follows a Holling type II functional response. The attack rate a_{ij} and handling time h_{ik} are both mass- and temperature-dependent according to Rall et al. (2012) and Li et al. (2018).

$$a_{ik} = a_0 M_i^{s_a} \exp\left(\frac{-E_a}{k_B T}\right) \tag{S3-3a}$$

$$h_{ik} = h_0 M_i^{s_h} \exp\left(\frac{-E_h}{k_B T}\right) \tag{S3-3b}$$

M_i is predator's body mass, a_0 and h_0 are normalisation constants, s_a and s_h are the allometric scaling exponents, E_a and E_h are the activation energies, k_B is Boltzmann's constant ($k_B = 8.62 \times 10^{-5}\,\mathrm{eV\,K}^{-1}$) and T (K) is the temperature.

We used the data set gathered by Rall et al. (2012) and Li et al. (2018) (available at the following link: http://dx.doi.org/10.5061/dryad.g5516) and performed the same statistical analysis but we converted the units according to Table S3-6 (see Li et al. (2018) and their supporting information for more details). In addition to the variables seen in equations (S3-3a) and (S3-3b), Li et al. (2018) considered the dimensionality of the arena used for the experiment (2D or 3D), the duration of the experiment and the starvation state of the individuals used during the experiment. For our model, we consider only used the parameters calculated for a 2D environment and we dropped the duration and the starvation states from the statistical analysis since these variables are not modelled. Finally, we convert the individual attack rate into mass-specific attack rate.

Li et al. (2018) did not consider individuals as units when expressing their parameters but it is a mistake because prey individuals and predator individuals are not equivalent and this is critical when converting an individual based functional response into a biomass based functional response. We have corrected the units in Table S3-6. Then, to get biomass based parameters, we have to divide attack rates a_{ij} by predator body mass M_i and to multiply handling times h_{ik} by the ratio of predator to prey body mass M_i/M_j.

Table S3-6: Conversion of the units used in Li et al. (2018) to the units used in our model.

Parameter	Original value and units	Converted value and unites
a_{ij}	$\mathrm{m^2\,Ind_{pred}}^{-1}\,\mathrm{s}^{-1}$	$\mathrm{m^2\,mgC_{pred}}^{-1}\,\mathrm{d}^{-1}$
a_0	$\exp(-10.59)\,\mathrm{m^2\,Ind_{pred}}^{-1}\,\mathrm{s}^{-1}\,\mathrm{mg_{pred}}^{-s_a}$	$4.67 \times 10^5\,\mathrm{m^2\,d}^{-1}\,\mathrm{mgC_{pred}}^{-1-s_a}$
s_a	0.49	-0.49
E_a	0.43 eV	0.43 eV
h_{ik}	$\mathrm{s\,Ind_{pred}\,mg_{prey}}^{-1}$	$\mathrm{d\,mgC_{pred}\,mgC_{prey}}^{-1}$
h_0	$\exp(13.01)\,\mathrm{s\,Ind_{pred}\,Ind_{prey}}^{-1}\,\mathrm{mg}^{-s_h}$	$7.22 \times 10^{-6}\,\mathrm{d\,mgC_{pred}\,mgC_{prey}}^{-1}\,\mathrm{mgC}^{-s_h}$
s_h	-0.73	0.24
E_h	−0.3 eV	−0.31 eV
M_i	mg (fresh)	mgC

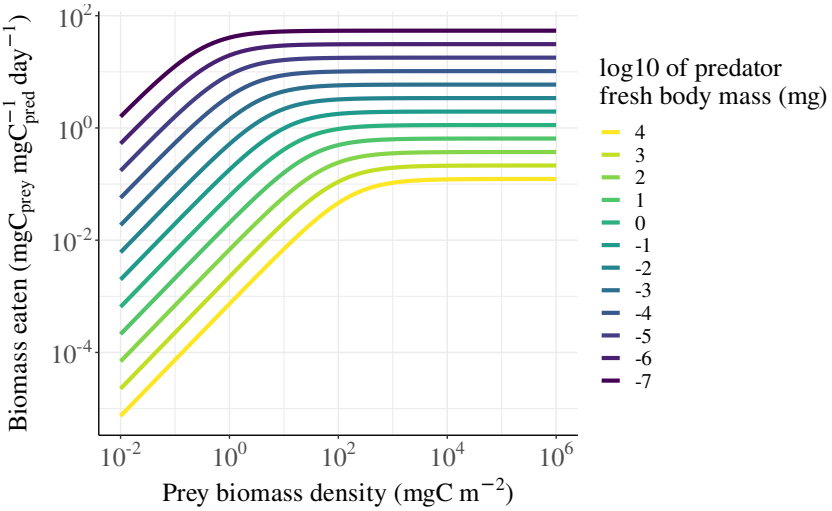

Figure S3-4: Functional response of carnivores (biomass of prey eaten per unit of predator biomass per day) depending on predator fresh body mass.

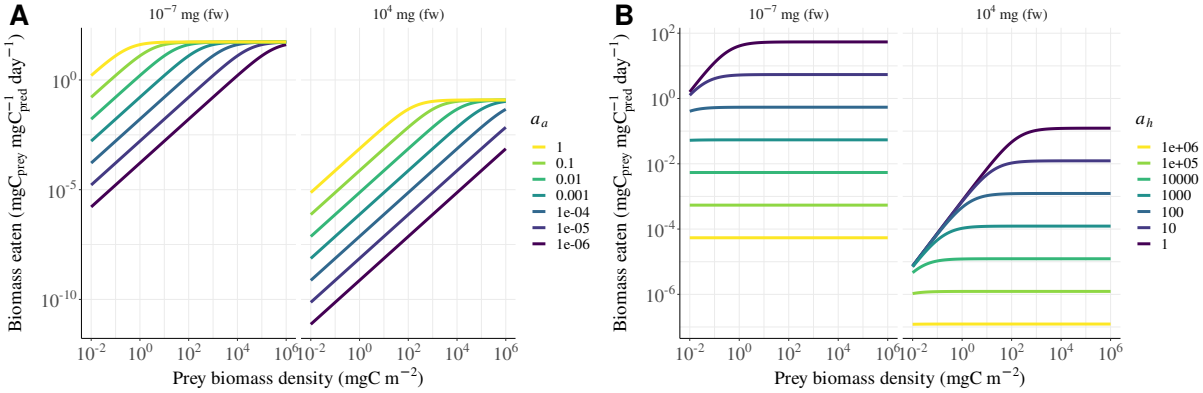

Figure S3-5: Functional response of carnivores (biomass of prey eaten per unit of predator biomass per day) depending on predator fresh body mass and parameters a_a and a_h tuning ther attack rate and the handling time. Two body masses of predators are tested.

S3-7 Microbe unit conversion

The kinetic of nutrient uptake and organic matter decomposition are not known in detail in the bulk of soil while the Michaelis-Menten kinetics have been well described in water. Since soil bacteria live in the thin layer of water covering soil particles, we can link the water concentration of nutrient (mg L^{-1}) to the soil content of nutrient (mg m^{-2}) thanks to soil moisture. Therefore, we consider a parallelepiped of $1 \times 1 \times 0.1$ m whose moisture represents 20% of soil volume (usually, moisture ranges between 10% and 30% (Heathman et al., 2003)).

German et al. (2012) originally defined half-saturation constant K_C and maximal absorption rate φ_C^{max} as functions of temperature based on the measurement of enzymatic activity (β-glucosidase extracted from 1 g of soil degrading 4-MUB-β-D-glucopyranoside $C_{16}H_{18}O_8$ but only C_6 are degraded in the substrate, the rest being the fluorescent dye):

$$K_C = a_{K_C} \exp(K_{slope} T + K_{int}) \tag{S3-4a}$$
$$\varphi_C^{max} = a_{\varphi_C} \exp(\varphi_{slope} T + \varphi_{int}) \tag{S3-4b}$$

K_{slope}, φ_{slope}, K_{int} and φ_{int} are regression coefficients and intercepts. T is the temperature (°C). a_{K_C} and a_φ are tuning coefficient ensuring the conversion of the enzymatic activity into bacterial activity. However, the units of their parameters are wrong because the resultant of the terms inside the exponential must be dimensionless. Then, we rewrite equations (S3-4a) and (S3-4b) to set correct units:

$$K_C = a_{K_C} K_{C0} \exp(s_{K_C} T) \tag{S3-5a}$$
$$\varphi_C^{max} = a_{\varphi_C} \varphi_{C0} \exp(s_{\varphi_C} T) \tag{S3-5b}$$

$s_{K_C} = K_{slope}$, $s_{\varphi_C} = \varphi_{slope}$, $K_{C0} = \exp(K_{int} - s_{K_C} T_0)$ and $\varphi_{C0} = \exp(\varphi_{int} - s_{varphi_C} T_0)$, with $T_0 = 273.15\,\mathrm{K}$. Because German et al. (2012) strongly relied on tuning parameters to calibrate their model, we decided to use the values of FOM and SOM consumption rates measured at $T = 20\,^\circ\mathrm{C}$ by Perveen et al. (2014) for our own calibration. The consumption of organic matter does not depend on FOM and SOM stocks in Perveen et al.'s (2014) model, which then corresponds to the maximum uptake rate of the Michaelis-Menten function. Then, we solve the following equation:

$$\varphi_{Perveen} = \varphi_{C0} \exp(s_{\varphi_C} T_{=293.15K}) \tag{S3-6}$$

The kinetic of mineral nitrogen and dissolved organic carbon (DOC) are calculated from the values used by Grover (2003). However, the their parameters do not depend on temperature and, for the sake of consistency, we will consider the same temperature dependency as organic matter decomposition. We will consider that the values of half-saturations and maximum uptake rates have been measured at $T = 20\,^\circ\mathrm{C}$ and the cell wet mass is roughly $1 \times 10^{-9}\,\mathrm{mg}$ (Makarieva et al., 2005).

Table S3-7: Conversion of the units related to microbe nutrition. The original values of $K_{.0}$ and $\varphi_{.0}$ are the values of $K_.$ and $\varphi_.^{max}$ for the parameters from Grover (2003) and Perveen et al. (2014).

Parameter	Original value and units	Converted value and unites	Reference
K_{N0}	$1 \times 10^{-4}\,\mathrm{mol\,m^{-3}}$	$1.3 \times 10^{-6}\,\mathrm{mgN\,m^{-2}}$	Grover, 2003
K_{DOC0}	$1 \times 10^{-3}\,\mathrm{mol\,m^{-3}}$	$1.1 \times 10^{-5}\,\mathrm{mgC\,m^{-2}}$	Grover, 2003
K_{C0} (FOM, SOM)	$24.3\,\mu\mathrm{mol\,L^{-1}}$	$3.2 \times 10^{-3}\,\mathrm{mgC\,m^{-2}}$	German et al., 2012
φ_{N0}	$7.7 \times 10^{-15}\,\mathrm{mol\,cell^{-1}\,d^{-1}}$	$1.22 \times 10^{-8}\,\mathrm{mgN\,mgC^{-1}\,d^{-1}}$	Grover, 2003
φ_{C0} (DOC)	$52 \times 10^{-15}\,\mathrm{mol\,cell^{-1}\,d^{-1}}$	$7.09 \times 10^{-8}\,\mathrm{mgC\,mgC^{-1}\,d^{-1}}$	Grover, 2003
φ_{C0} (FOM)	$0.0093\,\mathrm{d^{-1}}$	$8.87 \times 10^{-11}\,\mathrm{d^{-1}}$	Perveen et al., 2014
φ_{C0} (SOM)	$0.0318\,\mathrm{d^{-1}}$	$3.03 \times 10^{-10}\,\mathrm{d^{-1}}$	Perveen et al., 2014
s_{K_N}	-	$0.034\,\mathrm{K^{-1}}$	assumed
$s_{K_{DOC}}$	-	$0.034\,\mathrm{K^{-1}}$	assumed
s_{K_C} (FOM, SOM)	$0.034\,^\circ\mathrm{C^{-1}}$	$0.034\,\mathrm{K^{-1}}$	German et al., 2012
s_{φ_N}	-	$0.063\,\mathrm{K^{-1}}$	assumed
$s_{\varphi_{DOC}}$	-	$0.063\,\mathrm{K^{-1}}$	assumed
s_{φ_C} (FOM, SOM)	$0.063\,^\circ\mathrm{C^{-1}}$	$0.063\,\mathrm{K^{-1}}$	German et al., 2012

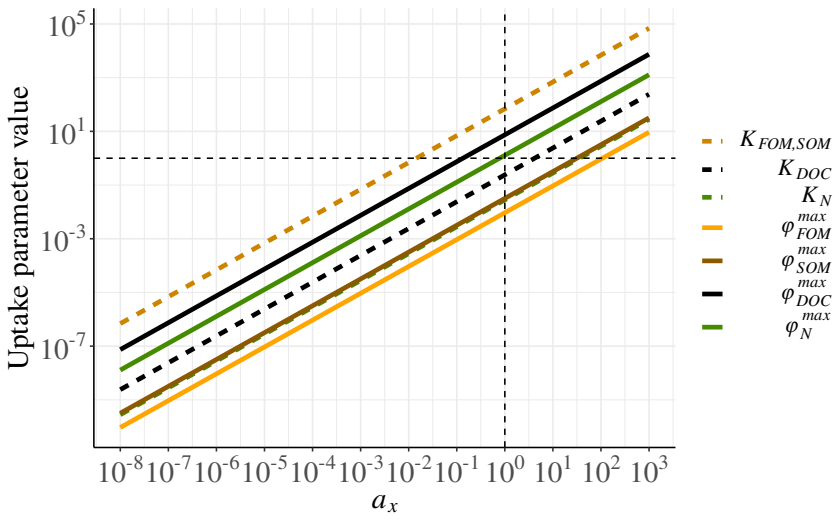

Figure S3-6: Selection of tuning parameters a_x.

S3-8 Faeces geometry calculation

Detritus D_i are modelled by spheres of radius r_i, which is calculated from the specific area (assumed to be discs) of the faeces of soil invertebrates photographed by Ganault et al. (2022) (available by direct communication). Specific faeces area ($mm^2\,g^{-1}$) was measured by calculating the projected surface area of 10 faecal pellets from photographs using a stereo-microscope and reporting it to their total dry mass. Thus, the individual area of a single pellet is calculated by dividing the specific area by the average dry weight of faecal pellets. We identify a linear relationship between pellet radius and organism fresh body mass. However, we discriminate two class of invertebrates depending on their body shape: compact organisms (Fig. S3-8A,B,D,F) and elongated organisms (Fig. S3-8C,E), which produce smaller faecal pellets compared to their body mass due to their reduced body section. For the sake of generality, we keep the parameters relative to compact body shape.

$$r_i = r_{int} + r_{slope} M_i \tag{S3-7}$$

The relationship between invertebrate body mass and the mass of their faeces is not significant due to the very high dispersion of data points. Since found a significant relationship between invertebrate body mass and faeces radius, we could explain the variability of faeces mass by a variability of their density. In the model, we use body mass as a proxy of body size to assess the possible interactions and not to directly calculate flows of matter and energy. Thus, we just calculate the general ratio between invertebrate fresh body mass M_i and faeces fresh mass M_{D_i} to estimate the rough mass of the faeces of each of our modelled organism.

$$M_{D_i}/M_i = 0.047 \tag{S3-8}$$

Table S3-8: Result of the ANOVA testing the effect of body mass and body shape on the radius of faeces. Fixed and cross-effects are significant.

	Sum Sq	Df	F-value	p-value
body mass	136.74	1	12.51	1.5×10^{-3}
body shape	554.62	1	50.74	1.5×10^{-7}
body mass × body shape	67.26	1	6.15	0.02

Table S3-9: Values of the parameters from equation (S2-4).

Parameter	Compact	Elongated	Units
r_{int}	9.81	8.60	µm
r_{slope}	0.87	0.22	µm mgC^{-1}

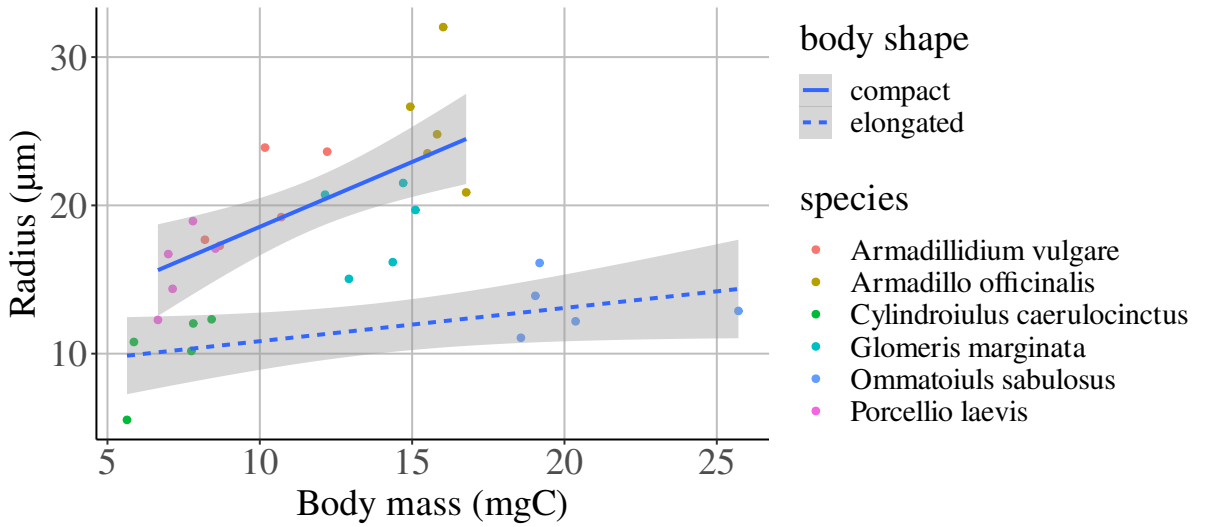

Figure S3-7: Linear regression of the radius (µm) of faeces pellets (represented as spheres) depending on fresh body mass (mg) and body shape ($r^2 = 0.7036$).

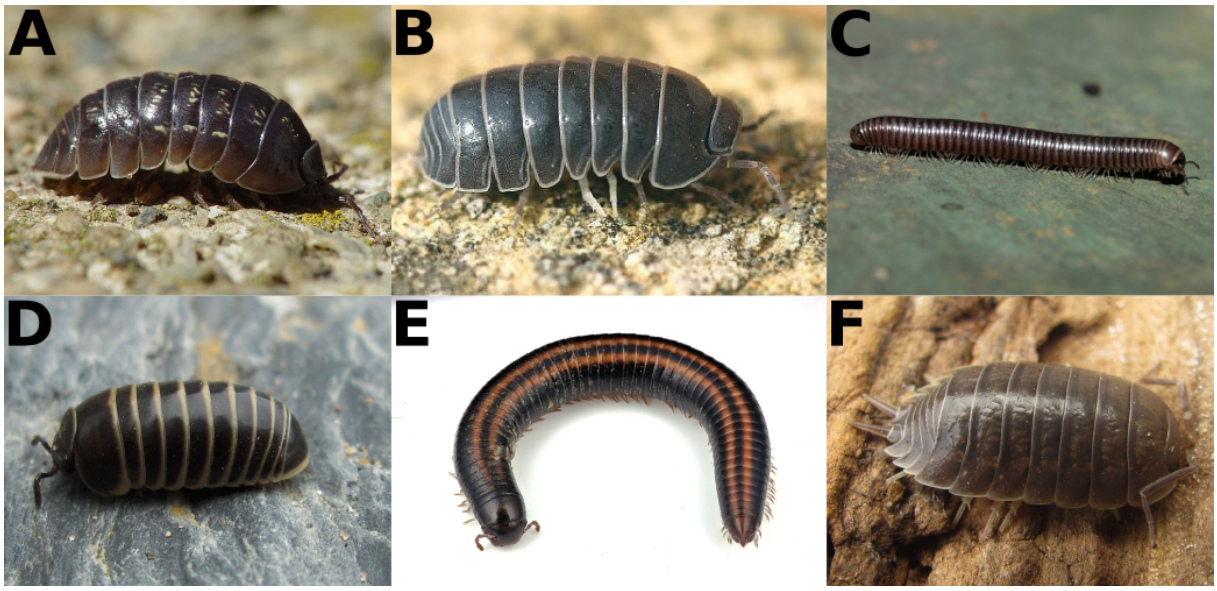

Figure S3-8: Invertebrates whose faeces characteristics have been measured by Ganault et al. (2022). **A)** *Armadillidium vulgare* **B)** *Armadillo officinalis* **C)** *Cylindroiulus caerulocinctus* **D)** *Glomeris marginata* **E)** *Ommatoiuls sabulosus* **F)** *Porcellio laevis.*

S3-9 Environmental parameter conversion

For the conversion from bulk soil to soil volume, we use the measure made by Bowden et al. (2014) : $1\,\mathrm{g\,cm^{-3}}$. We assume that the leaching rate of DOC ℓ_{DOC} is equal to the leaching rate of mineral nitrogen ℓ_N. The maximum transition rate of microbes between active and dormant states (and vice versa) has been calculated by Stolpovsky et al., 2011 by fitting a bacteria population model on experimental data obtained with *Pseudomonas putida.*

The input of DOC corresponds to the gross rhizodeposition, which represents roughly 10% of the net primary production (Jones et al., 2004; Pausch and Kuzyakov, 2018).

The data relative to the various stocks of carbon presented in Table 1a are taken from Xu et al. (2013). Since we consider global patterns, we took the total values in Table 4 for in their main text for the microbial C and divided it by the total area. Then, the SOM pool is evaluated thanks to the global average C_{mic}/C_{org} ratio in Table 2 (1.2%) and the assumption that C_{org}=C_{mic}+C_{SOM} (*i.e.* the organic compartment consists in living and dead matter). Therefore, we get:

$$C_{SOM} = C_{mic}(1/0.012 - 1) \tag{S3-9}$$

The data relative to the FOM stock were taken from Heděnec et al. (2022) (available in their supporting information), averaged over biomes and converted into carbon with the dry to carbon mass ratio 0.42 from Andrieux et al. (2021).

Table S3-10: Conversion of the units related to nonallometric parameters.

Parameter	Original value and units	Converted value and unites	Reference
I_N	$0.063\,\mathrm{gN\,m^{-2}\,d^{-1}}$	$63\,\mathrm{mgN\,m^{-2}\,d^{-1}}$	Perveen et al., 2014
I_{DOC} (meadow)	0.1 to $5\,\mathrm{gC\,kg^{-1}\,month^{-1}}$	33.33 to $1666.7\,\mathrm{mgC\,m^{-2}\,d^{-1}}$	Jones et al., 2009
I_{FOM} (forest)	$239\,\mathrm{gC\,m^{-2}\,yr^{-1}}$	$655\,\mathrm{mgC\,m^{-2}\,d^{-1}}$	Bowden et al., 2014
I_{FOM} (coniferous)	111 to $667\,\mathrm{gC\,m^{-2}\,yr^{-1}}$	304.1 to $1827.4\,\mathrm{mgC\,m^{-2}\,d^{-1}}$	Wunderlich et al., 2012
I_{FOM} (deciduous)	206 to $447\,\mathrm{gC\,m^{-2}\,yr^{-1}}$	564.4 to $1224.7\,\mathrm{mgC\,m^{-2}\,d^{-1}}$	Wunderlich et al., 2012
ℓ_N	$2.6 \times 10^{-3}\,\mathrm{d^{-1}}$	$2.6 \times 10^{-3}\,\mathrm{d^{-1}}$	Perveen et al., 2014
ℓ_{DOC}	-	$2.6 \times 10^{-3}\,\mathrm{d^{-1}}$	assumed
ℓ_{FOM}	-	$1 \times 10^{-3}\,\mathrm{d^{-1}}$	assumed
ℓ_{SOM}	-	$1 \times 10^{-3}\,\mathrm{d^{-1}}$	assumed
Q	$1\,\mathrm{h^{-1}}$	$24\,\mathrm{d^{-1}}$	Stolpovsky et al., 2011

Table S3-11: FOM input (litterfall) across biomes (Heděnec et al., 2022). FOM input ranges from 22 to $783\,\mathrm{mgC\,m^{-2}\,d^{-1}}$.

Biome	Original ($\mathrm{kg\,ha^{-1}\,yr^{-1}}$)	SE	Converted ($\mathrm{mgC\,m^{-2}\,d^{-1}}$)	SE
Tundra and cold steppe	1702	706	196	81
Boreal forest	2032	1094	234	126
Temperate forest	3221	1394	371	160
Temperate grassland	2997	1053	345	121
Mediterranean vegetation	2974	1480	342	170
Desert	638	448	73	52
Tropical grassland	3893	1894	448	218
Tropical forest	5413	1394	623	160

Table S3-12: DOC input (rhizodeposition) across biomes assumed to be equivalent to 10% of the net primary production (Melillo et al., 1993). SOM input ranges from X to $1\,\mathrm{mgC\,m^{-2}\,d^{-1}}$.

Biome	NPP ($\mathrm{gC\,m^{-2}\,yr^{-1}}$)	Rhizodeposition ($\mathrm{mgC\,m^{-2}\,d^{-1}}$)
Tundra	120	33
Boreal forest	238	65
Temperate forest	620	170
Temperate grassland	335	92
Desert	53	15
Tropical grassland	335	108
Tropical forest	1098	300
Mediterranean	343	94

References

Andrieux, B., Signor, J., Guillou, V., Danger, M., & Jabot, F. (2021). Body stoichiometry of heterotrophs: Assessing drivers of interspecific variations in elemental composition (A. Bjorkman, Ed.). *Global Ecology and Biogeography*, *30*(4), 883–895. https://doi.org/10.1111/geb.13265

Beddington, J. R. (1975). Mutual interference between parasites or predators and its effect on searching efficiency. *The Journal of Animal Ecology*, *44*(1), 331. https://doi.org/10.2307/3866

Bowden, R. D., Deem, L., Plante, A. F., Peltre, C., Nadelhoffer, K., & Lajtha, K. (2014). Litter input controls on soil carbon in a temperate deciduous forest. *Soil Science Society of America Journal*, *78*(S1). https://doi.org/10.2136/sssaj2013.09.0413nafsc

Brose, U., Jonsson, T., Berlow, E. L., Warren, P., Banasek-Richter, C., Bersier, L.-F., Blanchard, J. L., Brey, T., Carpenter, S. R., Blandenier, M.-F. C., Cushing, L., Dawah, H. A., Dell, T., Edwards, F., Harper-Smith, S., Jacob, U., Ledger, M. E., Martinez, N. D., Memmott, J., … Cohen, J. E. (2006). Consumer–resource body-size relationships in natural food webs. *Ecology*, *87*(10), 2411–2417. https://doi.org/10.1890/0012-9658(2006)87[2411:CBRINF]2.0.CO;2

Brown, J. H., Gillooly, J. F., Allen, A. P., Savage, V. M., & West, G. B. (2004). Toward a metabolic theory of ecology. *Ecology*, *85*(7), 1771–1789. https://doi.org/10.1890/03-9000

Chown, S. L., Marais, E., Terblanche, J. S., Klok, C. J., Lighton, J. R. B., & Blackburn, T. M. (2007). Scaling of insect metabolic rate is inconsistent with the nutrient supply network model. *Functional Ecology*, *21*(2), 282–290. https://doi.org/10.1111/j.1365-2435.2007.01245.x

DeAngelis, D. L., Goldstein, R. A., & O'Neill, R. V. (1975). A model for tropic interaction. *Ecology*, *56*(4), 881. https://doi.org/10.2307/1936298

Ehnes, R. B., Rall, B. C., & Brose, U. (2011). Phylogenetic grouping, curvature and metabolic scaling in terrestrial invertebrates: Invertebrate metabolism. *Ecology Letters*, *14*(10), 993–1000. https://doi.org/10.1111/j.1461-0248.2011.01660.x

Fenchel, T., & Finlay, B. J. (1983). Respiration rates in heterotrophic, free-living protozoa. *Microbial Ecology*, *9*(2), 99–122. https://doi.org/10.1007/BF02015125

Ferris, H., Lau, S., & Venette, R. (1995). Population energetics of bacterial-feeding nematodes: Respiration and metabolic rates based on CO2 production. *Soil Biology and Biochemistry*, *27*(3), 319–330. https://doi.org/10.1016/0038-0717(94)00186-5

Ganault, P., Barantal, S., Coq, S., Hättenschwiler, S., Lucas, S., Decaëns, T., & Nahmani, J. (2022). Leaf litter morphological traits, invertebrate body mass and phylogenetic affiliation explain the feeding and feces properties of saprophagous macroarthropods. *European Journal of Soil Biology*, *109*, 103383. https://doi.org/10.1016/j.ejsobi.2021.103383

German, D. P., Marcelo, K. R. B., Stone, M. M., & Allison, S. D. (2012). The Michaelis-Menten kinetics of soil extracellular enzymes in response to temperature: A cross-latitudinal study. *Global Change Biology*, *18*(4), 1468–1479. https://doi.org/10.1111/j.1365-2486.2011.02615.x

Grover, J. P. (2003). The impact of variable stoichiometry on predator–prey interactions: A multinutrient approach. *The American Naturalist*, *162*(1), 29–43. https://doi.org/10.1086/376577

Harfoot, M. B. J., Newbold, T., Tittensor, D. P., Emmott, S., Hutton, J., Lyutsarev, V., Smith, M. J., Scharlemann, J. P. W., & Purves, D. W. (2014). Emergent global patterns of ecosystem structure and function from a mechanistic general ecosystem model (M. Loreau, Ed.). *PLoS Biology*, *12*(4), e1001841. https://doi.org/10.1371/journal.pbio.1001841

Heathman, G. C., Starks, P. J., Ahuja, L. R., & Jackson, T. J. (2003). Assimilation of surface soil moisture to estimate profile soil water content. *Journal of Hydrology*, *279*(1-4), 1–17. https://doi.org/10.1016/S0022-1694(03)00088-X

Heděnec, P., Jiménez, J. J., Moradi, J., Domene, X., Hackenberger, D., Barot, S., Frossard, A., Oktaba, L., Filser, J., Kindlmann, P., & Frouz, J. (2022). Global distribution of soil fauna functional groups and their estimated litter consumption across biomes. *Scientific Reports*, *12*(1), 17362. https://doi.org/10.1038/s41598-022-21563-z

Johnston, A. S. A., & Sibly, R. M. (2018). The influence of soil communities on the temperature sensitivity of soil respiration. *Nature Ecology & Evolution*, *2*(10), 1597–1602. https://doi.org/10.1038/s41559-018-0648-6

Jones, D. L., Nguyen, C., & Finlay, R. D. (2009). Carbon flow in the rhizosphere: Carbon trading at the soil–root interface. *Plant and Soil*, *321*(1-2), 5–33. https://doi.org/10.1007/s11104-009-9925-0

Jones, D. L., Hodge, A., & Kuzyakov, Y. (2004). Plant and mycorrhizal regulation of rhizodeposition. *New Phytologist*, *163*(3), 459–480. https://doi.org/10.1111/j.1469-8137.2004.01130.x

Klekowski, R., Wasilewska, L., & Paplinska, E. (1972). Oxygen consumption by soil-inhabiting nematodes. *Nematologica*, *18*(3), 391–403. https://doi.org/10.1163/187529272X00665

Lampert, W. (1984). *A Manual on methods for the assessment of secondary productivity in fresh waters* (J. A. Downing & F. H. Rigler, Eds.; 2nd ed). Blackwell Scientific Publications ; Blackwell Mosby Book Distributors.

Lang, B., Ehnes, R. B., Brose, U., & Rall, B. C. (2017). Temperature and consumer type dependencies of energy flows in natural communities. *Oikos*, *126*(12), 1717–1725. https://doi.org/10.1111/oik.04419

Laybourn, J., & Finlay, B. J. (1976). Respiratory energy losses related to cell weight and temperature in ciliated protozoa. *Oecologia*, *24*(4), 349–355. https://doi.org/10.1007/BF00381141

Li, Y., Rall, B. C., & Kalinkat, G. (2018). Experimental duration and predator satiation levels systematically affect functional response parameters. *Oikos*, *127*(4), 590–598. https://doi.org/10.1111/oik.04479

Makarieva, A. M., Gorshkov, V. G., & Li, B.-L. (2005). Energetics of the smallest: Do bacteria breathe at the same rate as whales? *Proceedings of the Royal Society B: Biological Sciences*, *272*(1577), 2219–2224. https://doi.org/10.1098/rspb.2005.3225

Manzoni, S., Schaeffer, S., Katul, G., Porporato, A., & Schimel, J. (2014). A theoretical analysis of microbial eco-physiological and diffusion limitations to carbon cycling in drying soils. *Soil Biology and Biochemistry*, *73*, 69–83. https://doi.org/10.1016/j.soilbio.2014.02.008

McCoy, M. W., & Gillooly, J. F. (2008). Predicting natural mortality rates of plants and animals. *Ecology Letters*, *11*(7), 710–716. https://doi.org/10.1111/j.1461-0248.2008.01190.x

Meehan, T. D. (2006). Mass and temperature dependence of metabolic rate in litter and soil invertebrates. *Physiological and Biochemical Zoology*, *79*(5), 878–884. https://doi.org/10.1086/505997

Melillo, J. M., McGuire, A. D., Kicklighter, D. W., Moore, B., Vorosmarty, C. J., & Schloss, A. L. (1993). Global climate change and terrestrial net primary production. *Nature*, *363*(6426), 234–240. https://doi.org/10.1038/363234a0

Nielsen, C. O. (1961). Respiratory metabolism of some populations of enchytraeid worms and freeliving nematodes. *Oikos*, *12*(1), 17. https://doi.org/10.2307/3565169

Panikov, N. S., & Sizova, M. V. (1996). A kinetic method for estimating the biomass of microbial functional groups in soil. *Journal of Microbiological Methods*, *24*(3), 219–230. https://doi.org/10.1016/0167-7012(95)00074-7

Pausch, J., & Kuzyakov, Y. (2018). Carbon input by roots into the soil: Quantification of rhizodeposition from root to ecosystem scale. *Global Change Biology*, *24*(1), 1–12. https://doi.org/10.1111/gcb.13850

Perveen, N., Barot, S., Alvarez, G., Klumpp, K., Martin, R., Rapaport, A., Herfurth, D., Louault, F., & Fontaine, S. (2014). Priming effect and microbial diversity in ecosystem functioning and response to global change: A modeling approach using the SYMPHONY model. *Global Change Biology*, *20*(4), 1174–1190. https://doi.org/10.1111/gcb.12493

Peters, R. H. (1983). *The ecological implications of body size*. Cambridge University Press. Retrieved March 12, 2015, from http://ebooks.cambridge.org/ref/id/CBO9780511608551

Pollierer, M. M., Langel, R., Körner, C., Maraun, M., & Scheu, S. (2007). The underestimated importance of belowground carbon input for forest soil animal food webs. *Ecology Letters*, *10*(8), 729–736. https://doi.org/10.1111/j.1461-0248.2007.01064.x

Potapov, A. M., Beaulieu, F., Birkhofer, K., Bluhm, S. L., Degtyarev, M. I., Devetter, M., Goncharov, A. A., Gongalsky, K. B., Klarner, B., Korobushkin, D. I., Liebke, D. F., Maraun, M., Mc Donnell, R. J., Pollierer, M. M., Schaefer, I., Shrubovych, J., Semenyuk, I. I., Sendra, A., Tuma, J., … Scheu, S. (2022). Feeding habits and multifunctional classification of soil-associated consumers from protists to vertebrates. *Biological Reviews*, brv.12832. https://doi.org/10.1111/brv.12832

Potapov, A. M., Rozanova, O. L., Semenina, E. E., Leonov, V. D., Belyakova, O. I., Bogatyreva, V. Y., Degtyarev, M. I., Esaulov, A. S., Korotkevich, A. Y., Kudrin, A. A., Malysheva, E. A., Mazei, Y. A., Tsurikov, S. M., Zuev, A. G., & Tiunov, A. V. (2021). Size compartmentalization of energy channeling in terrestrial belowground food webs. *Ecology*, *102*(8). https://doi.org/10.1002/ecy.3421

Rall, B. C., Brose, U., Hartvig, M., Kalinkat, G., Schwarzmuller, F., Vucic-Pestic, O., & Petchey, O. L. (2012). Universal temperature and body-mass scaling of feeding rates. *Philosophical Transactions of the Royal Society B: Biological Sciences*, *367*(1605), 2923–2934. https://doi.org/10.1098/rstb.2012.0242

Schwarzmüller, F., Eisenhauer, N., & Brose, U. (2015). 'Trophic whales' as biotic buffers: Weak interactions stabilize ecosystems against nutrient enrichment (E. O'Gorman, Ed.). *Journal of Animal Ecology*, *84*(3), 680–691. https://doi.org/10.1111/1365-2656.12324

Stolpovsky, K., Martinez-Lavanchy, P., Heipieper, H. J., Van Cappellen, P., & Thullner, M. (2011). Incorporating dormancy in dynamic microbial community models. *Ecological Modelling*, *222*(17), 3092–3102. https://doi.org/10.1016/j.ecolmodel.2011.07.006

Wang, G., Mayes, M. A., Gu, L., & Schadt, C. W. (2014). Representation of dormant and active microbial dynamics for ecosystem modeling (J. H. Badger, Ed.). *PLoS ONE*, *9*(2), e89252. https://doi.org/10.1371/journal.pone.0089252

Wieder, W. R., Grandy, A. S., Kallenbach, C. M., & Bonan, G. B. (2014). Integrating microbial physiology and physio-chemical principles in soils with the MIcrobial-MIneral Carbon Stabilization (MIMICS) model. *Biogeosciences*, *11*(14), 3899–3917. https://doi.org/10.5194/bg-11-3899-2014

Wunderlich, S., Schulz, C., Grimmeisen, W., & Borken, W. (2012). Carbon fluxes in coniferous and deciduous forest soils. *Plant and Soil*, *357*(1-2), 355–368. https://doi.org/10.1007/s11104-012-1158-y

Xu, X., Thornton, P. E., & Post, W. M. (2013). A global analysis of soil microbial biomass carbon, nitrogen and phosphorus in terrestrial ecosystems: Global soil microbial biomass C, N and P. *Global Ecology and Biogeography*, *22*(6), 737–749. https://doi.org/10.1111/geb.12029